Neuron

An excitatory projection from the basal forebrain to the ventral tegmental area that underlies anorexia-like phenotypes

Graphical abstract

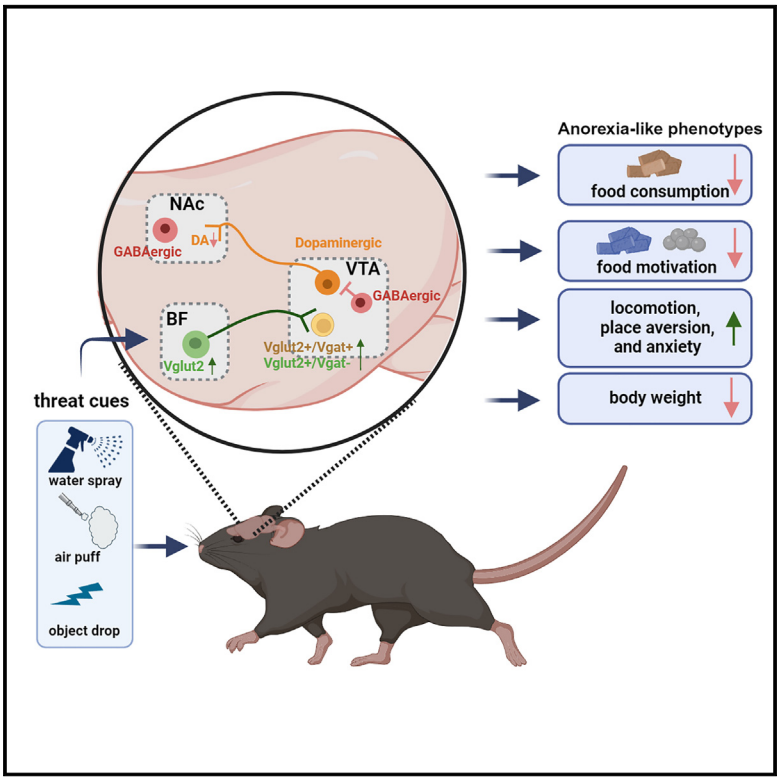

Highlights

- VTA^{Vglut2} neurons present the major VTA downstream target of BF^{Vglut2} neurons
- The BF^{Vglut2} → VTA^{Vglut2} circuit responds to threat cues
- Activation of the BF^{Vglut2} → VTA^{Vglut2} circuit induces anorexia-like phenotypes
- Activation of the BF^{Vglut2} → VTA^{Vglut2} circuit reduces dopamine release

Authors

Jing Cai, Yanyan Jiang, Yuanzhong Xu, ..., Yong Xu, Benjamin R. Arenkiel, Qingchun Tong

Correspondence

arenkiel@bcm.edu (B.R.A.), qingchun.tong@uth.tmc.edu (Q.T.)

In brief

Through combined circuit tracing, *in vivo* fiber photometry recording, and mouse genetics and behavioral studies, Cai et al. identified a glutamatergic circuit from the basal forebrain to VTA glutamatergic neurons, activation of which led to anorexia-like phenotypes. They observed that the hypophagia phenotype was accompanied by reduced dopamine release.

Cai et al., 2024, Neuron *112*, 458–472
February 7, 2024
https://doi.org/10.1016/j.neuron.2023.11.001

CellPress

CellPress

Neuron

Article

An excitatory projection from the basal forebrain to the ventral tegmental area that underlies anorexia-like phenotypes

Jing Cai,[1,2] Yanyan Jiang,[1] Yuanzhong Xu,[1] Zhiying Jiang,[1] Claire Young,[1] Hongli Li,[1] Joshua Ortiz-Guzman,[3] Yizhou Zhuo,[4] Yulong Li,[4] Yong Xu,[5] Benjamin R. Arenkiel,[3,5,*] and Qingchun Tong[1,2,6,7,*]

[1]Brown Foundation of Molecular Medicine for the Prevention of Human Diseases of McGovern Medical School, University of Texas Health Science Center at Houston, Houston, TX 77030, USA

[2]MD Anderson Cancer Center & UTHealth Graduate School for Biomedical Sciences, University of Texas Health Science at Houston, Houston, TX 77030, USA

[3]Department of Molecular and Human Genetics and Department of Neuroscience, Baylor College of Medicine, and Jan and Dan Duncan Neurological Research Institute, Texas Children's Hospital, Houston, TX 77030, USA

[4]State Key Laboratory of Membrane Biology, Peking University School of Life Sciences, PKU-IDG/McGovern Institute for Brain Research, Beijing 100871, China

[5]USDA/ARS Children's Nutrition Research Center, Department of Pediatrics, Baylor College of Medicine, One Baylor Plaza, Houston, TX 77030, USA

[6]Department of Neurobiology and Anatomy of McGovern Medical School, University of Texas Health Science Center at Houston, Houston, TX 77030, USA

[7]Lead contact

*Correspondence: arenkiel@bcm.edu (B.R.A.), qingchun.tong@uth.tmc.edu (Q.T.)

https://doi.org/10.1016/j.neuron.2023.11.001

SUMMARY

Maladaptation in balancing internal energy needs and external threat cues may result in eating disorders. However, brain mechanisms underlying such maladaptations remain elusive. Here, we identified that the basal forebrain (BF) sends glutamatergic projections to glutamatergic neurons in the ventral tegmental area (VTA) in mice. Glutamatergic neurons in both regions displayed correlated responses to various stressors. Notably, *in vivo* manipulation of BF terminals in the VTA revealed that the glutamatergic BF → VTA circuit reduces appetite, increases locomotion, and elicits avoidance. Consistently, activation of VTA glutamatergic neurons reduced body weight, blunted food motivation, and caused hyperactivity with behavioral signs of anxiety, all hallmarks of typical anorexia symptoms. Importantly, activation of BF glutamatergic terminals in the VTA reduced dopamine release in the nucleus accumbens. Collectively, our results point to overactivation of the glutamatergic BF → VTA circuit as a potential cause of anorexia-like phenotypes involving reduced dopamine release.

INTRODUCTION

With ever-changing environmental threat cues and internal nutritional checkpoints, an appropriate decision to engage in feeding behaviors is key to animal survival. Ongoing physical and perceived environmental disturbances can override internal energy needs and suppress feeding behaviors.[1,2] Maladaptation in balancing internal energy needs and external threat cues may result in anorexia or overeating, associated with debilitating malnutrition or obesity. In humans, heightened stress responses triggered by external cues reduce appetite and food motivation.[3,4] Specifically, in patients diagnosed with anorexia nervosa, an eating disorder with self-imposed starvation that has the highest mortality rate among mental disorders, there is a high prevalence of generalized anxiety disorders,[5,6] suggesting a profound impact of heightened stress responses on feeding behaviors. However, the brain circuits involved in sensing external stress cues to modulate feeding behaviors appropriately remain elusive.

In addition to its well-known functions in regulating arousal, wakefulness, learning, and memory, the basal forebrain (BF) has also been shown to sense environmental cues and process sensory input.[7–12] The BF contains cholinergic, gamma-aminobutyric acid (GABAergic), and glutamatergic neurons, and all these neuron groups respond to external stimuli.[9–11] Interestingly, recent results also suggest the importance of BF neurons in feeding regulation. BF GABAergic neurons promote food consumption and drive high-calorie food intake.[13,14] Loss of BF cholinergic neurons induces massive obesity due to increased food intake, whereas chronic activation of BF glutamatergic

(BF^{Vglut2}, i.e., expressing vesicular glutamate transporter 2) neurons leads to reduced food intake and starvation.[15,16] Notably, BF^{Vglut2} neurons respond to various sensory inputs, including odors with different valences, predator cues, and other physical threats associated with reduced feeding in animals.[15,17,18] These observations posit that the BF serves as a functional hub for sensing environmental cues, thus capable of profoundly impacting feeding behaviors.

The ventral tegmental area (VTA) is a well-studied dopamine (DA)-enriched midbrain structure involved in reward responses, motivation, learning, and memory.[19–21] Consistent with its role in reward consumption, the VTA has also been shown to modulate feeding, especially with respect to hedonic behaviors.[22] In particular, DA release from the VTA signals for a high-fat diet (HFD) intake and coincides with HFD-induced activity changes in hypothalamic agouti-related protein (AgRP) neurons, which have been established as key feeding regulatory neurons.[22–25] In particular, VTA DA neurons have been implicated in AgRP neuron function in linking hypophagia and locomotion.[26,27] In addition to DA neurons, the VTA also contains GABAergic and glutamatergic neurons, which have been shown to gate DA signals.[28–32] VTA GABAergic (VTA^{Vgat}, i.e., expressing vesicular GABA transporter) neurons form local connections with DA neurons to inhibit DA release and reduce reward consumption.[31–33] Similarly, VTA^{Vglut2} neurons send direct projections to various brain regions and local DA neurons[28,30] and play a complicated role in reward processing.[34–37] However, how VTA neurons integrate environmental cues to regulate feeding behaviors is unclear.

Here, we show that BF^{Vglut2} neurons send direct projections to the VTA, preferentially targeting VTA^{Vglut2} neurons. Both BF^{Vglut2} and VTA^{Vglut2} neurons responded to various environmental stimuli in a correlative manner. *In vivo* activation of the BF^{Vglut2} → VTA circuit inhibited feeding and led to behavioral avoidance. Activation of downstream VTA^{Vglut2} neurons led to hypophagia, diminished food motivation, hyperactivity, behavioral signs of anxiety, and body weight reduction, all resembling typical symptoms of anorexia. Furthermore, activation of this glutamatergic BF → VTA circuit was associated with reduced DA release in the nucleus accumbens (NAc), indicating a potential involvement of DA release in some of the observed anorexia-like phenotypes.

RESULTS

The BF sends glutamatergic projections to VTA^{Vglut2} neurons

We first aimed to identify the downstream targets of BF^{Vglut2} neurons. Given the preferential localization of ChR2 (channelrhodopsin 2) on cell membrane, ChR2 fused with a fluorescent reporter can be used to trace downstream projection sites.[38] To specifically target BF^{Vglut2} neurons, we used Vglut2-Cre, a mouse strain that expresses Cre from the Vglut2 (also named *Slc17a6*) locus,[39] and stereotaxically delivered conditional AAV5-Ef1a (elongation factor 1a promoter)-DIO (double-floxed inverted orientation)-ChR2-EYFP (enhanced yellow fluroscent protein) viral particles to the BF (Figures 1A, 1B, and S1A). Consistent with previous studies,[15,17] ChR2-EYFP-positive fibers were detected in the lateral habenula (LHb), the lateral hypothalamus (LH), and other brain regions (Figure S1B). Of note, we also found abundant EYFP-positive fibers in the VTA (Figure 1C). To verify the projection pattern, we performed retrograde adeno-associated viral (AAVrg)-based tracing experiments by injecting AAVrg-Ef1a-mCherry-IRES (internal ribosome entry site)-Flp (flippase) into the VTA,[40] and AAV-DJ8-hSyn (human synapsin 1)-Con/Fon-EYFP into the BF of Vglut2-Cre mice (Figures 1D–1F). Given that the AAV-DJ8-hSyn-Con/Fon-EYFP vector expresses EYFP in a Cre and Flp co-dependent manner, in this configuration, EYFP will selectively mark BF^{Vglut2} neurons that project to the VTA (Figure 1F). We found that EYFP-positive neuronal fibers were also present in the LHb in addition to the VTA (Figures 1G and 1H), suggesting that these VTA-projecting BF^{Vglut2} neurons send collateral projections to the LHb.

Given the heterogeneity of VTA neurons, we next sought to identify the neuronal subtype in the VTA that receives projections from BF^{Vglut2} neurons using the trans-synaptic tracer wheat germ agglutinin (WGA).[41] For this, we delivered conditional AAV-DJ8-DIO-WGA-EGFP viral particles to the BF of Vglut2-Cre mice (Figures 1I and 1J). The EGFP signals were traced from BF^{Vglut2} neurons to the VTA and further amplified by co-delivery of AAV1-Ef1a-Flp-DOG (dependent on GFP)-NW[42] and AAV1-Ef1a-fDIO-EYFP[40] in the VTA (Figures 1I and 1K). The AAV1-Ef1a-Flp-DOG-NW vector expresses Flp dependent on EGFP signals,[42] which, in this case, amplifies EGFP signals in VTA neurons that form synaptic contacts with BF^{Vglut2} neurons. AAV5-hSyn-DIO-mCherry was delivered to the VTA to visualize VTA^{Vglut2} neurons. As a result, abundant WGA-EGFP-labeled neurons, especially the majority of those in the anterior part of VTA, were co-localized with mCherry-positive glutamatergic neurons and mCherry-negative non-glutamatergic neurons (Figures 1K, S1C, and S1D). Specifically, with immunostaining for tyrosine hydroxylase (TH), we found a subset of TH neurons, especially in the caudal VTA, were positive for WGA (Figure S1E). Since WGA is known to be transported in both anterograde and retrograde fashions, some of the WGA-labeled VTA neurons might be the ones that project to BF^{Vglut2} neurons instead. We then used a nontoxic tetanus toxin C (TTC)-fragment-based trans-synaptic retrograde-tracing method[43] to identify VTA neurons that project to BF^{Vglut2} neurons. Toward this, we delivered AAV-DJ8-CAG-DIO-TTC-EGFP to the BF and a mixture of AAV1-Ef1a-Flp-DOG-NW and AAV5-fDIO-EYFP to the VTA of Vglut2-Cre mice (Figure S1F). We found that up to 60% of EYFP-labeled neurons, especially those in the caudal VTA, were TH-positive (Figures S1G and S1H), suggesting that a significant number of VTA TH neurons send projections to BF^{Vglut2} neurons.

To functionally identify downstream VTA neurons, we examined Fos expression in the VTA in response to photostimulation of BF^{Vglut2} neuron terminals. We injected the AAV8-DIO-mCherry virus into the VTA to label VTA^{Vglut2} neurons and TH immunostaining to identify DA neurons (Figures S2A and S2B). Although VTA^{Vglut2} neurons exhibited abundant Fos expression (Figure S2C), VTA TH neurons displayed minimal Fos expression upon photostimulation of the BF^{Vglut2} → VTA circuit (Figure S2D). We further quantitated the percentage of Fos neurons that are Vgat positive using the RNAscope *in situ* hybridization method

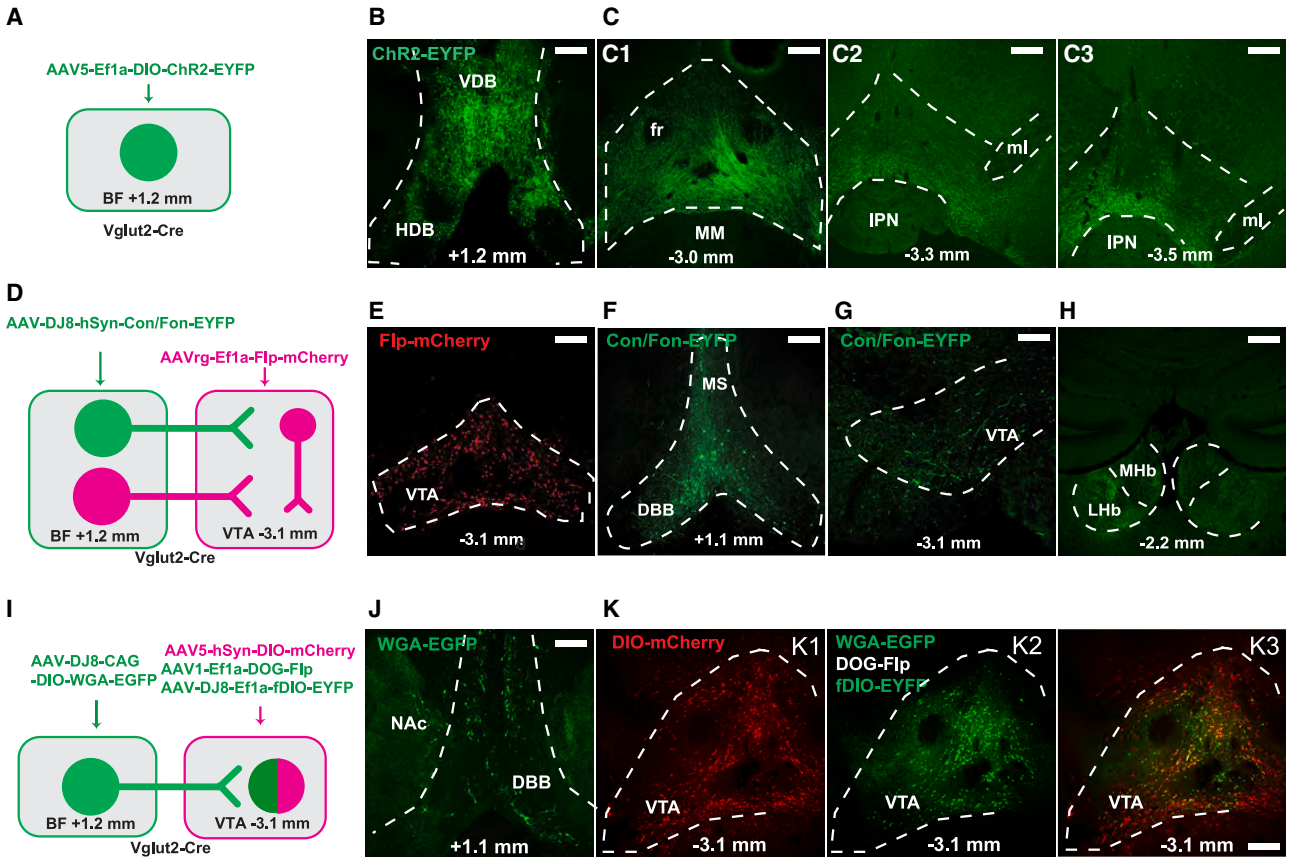

Figure 1. Direct projections from BF^{Vglut2} neurons to VTA^{Vglut2} neurons

(A) Schematic diagram showing virus injection strategies for labeling BF downstream glutamatergic neuronal fibers.
(B) Expression pattern of the injected ChR2 virus in the BF.
(C) Expression pattern of ChR2-EYFP within the anterior to posterior sections of the VTA.
(D) Schematic diagram showing virus injections to label BF^{Vglut2} neurons that send projections to the VTA.
(E) Expression pattern of the Flp-mCherry virus in the VTA.
(F) Expression pattern of the injected Con/Fon-EGFP virus in the BF. EGFP-labeled VTA-projecting BF^{Vglut2} neurons.
(G and H) EGFP-positive neuronal fibers from VTA-projecting BF^{Vglut2} neurons in the VTA (G) and the LHb (H).
(I) Schematic diagram showing virus injection strategies to label downstream VTA neurons that form synaptic connections with BF^{Vglut2} neurons.
(J) Expression pattern of the injected WGA-EGFP virus in the BF.
(K) Co-localization of EGFP-positive neurons and mCherry neurons (glutamatergic neurons). Scale bars, 200 μm. VDB, vertical diagonal band of broca; HDB, horizontal diagonal band of broca; Fr, fasciculus retroflexus; MM, mammillary nucleus; IPN, interpeduncular nucleus; Ml, medial mammillary nucleus, lateral.

(Figure S2E). A small portion of GABAergic neurons showed Fos expression (Figures S2F–S2H). These observations suggest that the major downstream target of BF^{Vglut2} neurons in the VTA expresses Vglut2, with a small portion also expressing Vgat, but not TH, and instead, DA neurons send projections back to the BF.

Emerging data suggest the existence of VTA^{Vglut2} neurons that express markers for GABAergic (Vgat), hereafter referred to as VTA$^{Vglut2+/Vgat+}$ neurons or TH (VTA$^{Vglut2+/TH+}$) neurons. To identify the subcategories of VTA^{Vglut2} neurons, we delivered AAV-DJ8-DIO-WGA-EGFP to the BF and a mixture of AAV1-Ef1a-Flp-DOG-NW and AAV8-Con/Fon-mCherry to the VTA of Vglut2-Cre mice (Figure S2I). In this configuration, mCherry will label WGA-traced VTA^{Vglut2} neurons. We then identified VTA^{Vgat} and TH neurons with RNAscope *in situ* against Vgat and TH immunostaining, respectively (Figure S2J), and our results showed that although a significant portion of VTA^{Vgat} neurons were co-localized with mCherry, i.e., glutamatergic neurons, a minimal amount of co-localization was observed between TH and mCherry (Figure S2K), confirming that it is unlikely that VTA$^{Vglut2+/TH+}$ neurons constitute the major downstream VTA neurons of BF^{Vglut2} neurons.

Given the fact that both VTA^{Vglut2} and VTA^{Vgat} neurons responded with Fos expression to the photostimulation of local BF^{Vglut2} neuron terminals, we employed ChR2-assisted circuit mapping (CRACM) to examine direct downstream neurons in the VTA (Figures S2L and S2N). Briefly, we delivered AAV5-Ef1a-DIO-ChR2-EYFP viral particles to the BF of Vglut2-Cre; Vgat-Flp mice and then delivered AAV5-hSyn-DIO-mCherry to the VTA to identify VTA^{Vglut2} neurons and AAV1-Ef1a-fDIO-EYFP[40] to label VTA^{Vgat} neurons. VTA$^{Vglut2+/Vgat+}$ neurons were EYFP and mCherry double-positive, and VTA$^{Vglut2-/Vgat+}$

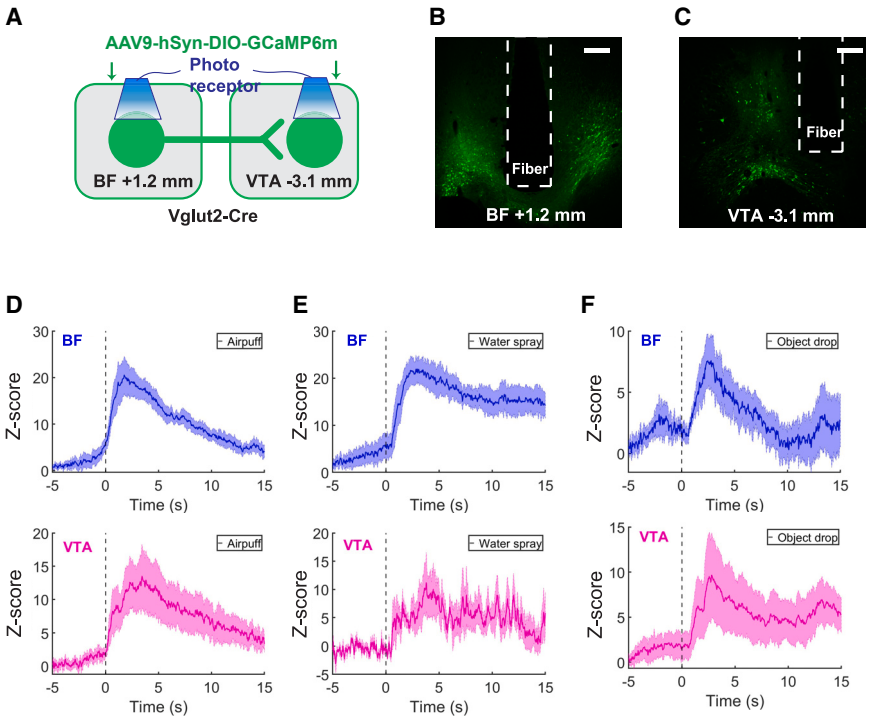

Figure 2. BF^{Vglut2} and VTA^{Vglut2} neurons showed correlated responses to external threat cues

(A) Schematic diagram showing virus injection and optic fiber cannulas implantation in both the BF and the VTA for simultaneous dual GCaMP6m-based fiber photometry recordings.

(B and C) Expression patterns of the injected GCaMP6m virus and cannula tracks in the BF (B) and the VTA (C). Scale bars, 200 μm.

(D–F) BF (top) and VTA (bottom) Ca^{2+} signal *Z* score in response to different physical stressors, including air puff (D), water spray (E), and object drop (F). Time = 0 represents the starting time of the stimuli. The shades represent ± SEM. Animals n = 7.

neurons were mCherry-positive only. We recorded time-locked excitatory postsynaptic currents (EPSCs) in the identified neurons elicited by photostimulation in brain slices. The recorded EPSCs were confirmed to be monosynaptic in nature with tetrodotoxin (TTX) and 4-aminopyridine (4-AP) (Figure S2M). Overall, 6 of the 19 VTA^{Vglut2} neurons (Figure S2M), 1 of the 11 VTA$^{Vglut2+/Vgat+}$ neurons (Figure S2O), and 0 of the 10 VTA$^{Vglut2-/Vgat+}$ neurons (Figure S2P) showed responses, suggesting that most of the downstream VTA targets of BF^{Vglut2} neurons are VTA$^{Vglut2+/Vgat-}$ and VTA$^{Vglut2+/Vgat+}$ neurons.

To better characterize VTA^{Vglut2}-projecting BF neurons, we next delivered AAV-DJ8-CAG-DIO-TTC-EGFP to the VTA and a mixture of AAV1-Ef1a-Flp-DOG-NW, AAV-DJ8-Ef1a-fDIO-EYFP, and AAV8-Ef1a-Con/Fon-mCherry[40] in the BF of Vglut2-Cre mice (Figures S1I and S1J). In this configuration, EYFP expression will identify BF neurons that project to VTA^{Vglut2} neurons, and mCherry expression will identify BF^{Vglut2} neurons that send direct projections to VTA^{Vglut2} neurons. Through this approach, we found that both BF^{Vglut2} and BF non-Vglut2 neurons were labeled (Figure S1J), suggesting that both groups send direct projections to VTA^{Vglut2} neurons. In addition, Con/Fon-mCherry-positive fibers from BF^{Vglut2} neurons that send projections to VTA^{Vglut2} neurons were also detected in other brain regions (Figures S1K and S1L), consistent with collateral projections of these neurons shown above.

Correlated responses of BF^{Vglut2} and VTA^{Vglut2} neurons to environmental cues

BF^{Vglut2} neurons respond to various environmental stimuli.[15] However, how these neurons transmit these signals to other brain regions is unknown. VTA^{Vglut2} neurons have also been shown to be sensitive to aversive stimuli.[36,44,45] To study the functional relationship between BF^{Vglut2} and VTA^{Vglut2} neurons in responding to environmental stressors, we performed genetically encoded calcium sensor 6m (GCaMP6m)-based *in vivo* dual-fiber photometry recordings in both groups of neurons in freely moving mice.[46] We delivered AAV9-hSyn-DIO-GCaMP6m viral particles to both the BF and the VTA of Vglut2-Cre mice and implanted optic cannulas independently targeting both areas (Figure 2A). The expression of GCaMP6m was confirmed in glutamatergic neurons of the BF and VTA (Figures 2B and 2C). As expected, BF^{Vglut2} neurons exhibited increased activity to air puff, water spray, and object drop (Figures 2D–2F). VTA^{Vglut2} neurons also exhibited increased activities similar to BF^{Vglut2} neurons (Figures 2D–2F). We further analyzed the correlation in activity peaks between BF^{Vglut2} neurons and VTA^{Vglut2} neurons during the periods of baseline non-stressed and stressed conditions. As expected, we found a strong correlation during stressed conditions (Figures S3B–S3D), which is consistent with a direct excitatory glutamatergic projection from the BF to VTA^{Vglut2} neurons. Surprisingly, we also found a strong but weaker correlation during the baseline non-stressed condition (Figure S3A), suggesting an active involvement of BF^{Vglut2} neurons to VTA^{Vglut2} neurons at baseline conditions and enhanced recruitment when animals are stressed.

Given both VTA$^{Vglut2+/Vgat-}$ and VTA$^{Vglut2+/Vgat+}$ neurons as downstream targets of BF^{Vglut2} neurons, we also examined *in vivo* activity responses of these neurons to photostimulation of BF^{Vglut2} neurons. We delivered AAV5-Ef1a-DIO-Chrimson-mCherry viral particles to the BF of Vglut2-Cre; Vgat-Flp mice and to the VTA with either AAV8-Con/Foff-GCaMP6f to target VTA$^{Vglut2+/Vgat-}$ neurons or AAV8-Con/Fon-GCaMP6f to target VTA$^{Vglut2+/Vgat+}$ neurons.[47,48] Then, at the same time, we implanted optic fiber cannulas to the BF for photostimulation and the VTA area for recording GCaMP6 signals (Figures S3E and S3H). Consistent with BF glutamatergic projections to the VTA, we observed an increase in the GCaMP6 signal from both VTA$^{Vglut2+/Vgat-}$ and VTA$^{Vglut2+/Vgat+}$ neurons

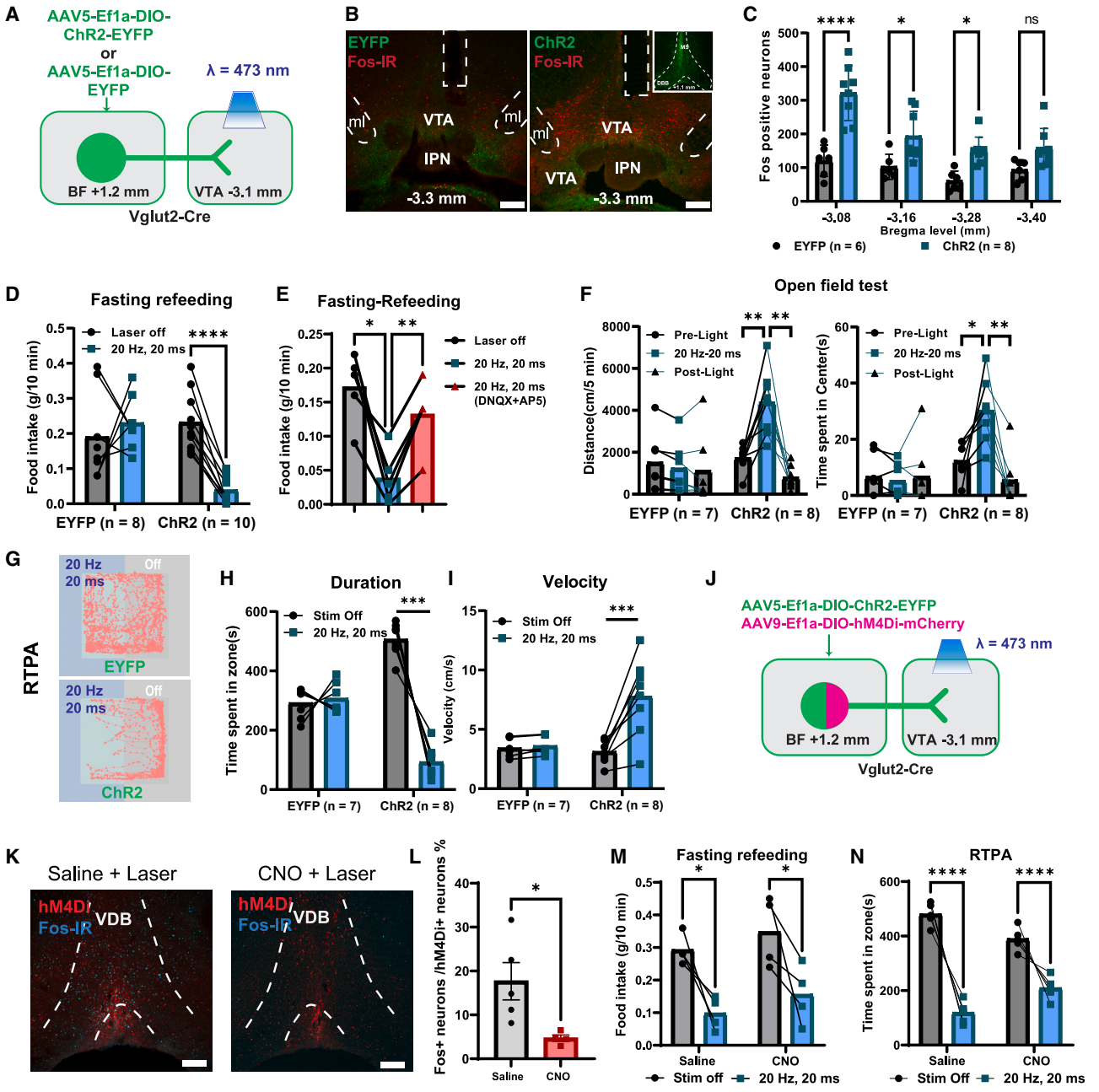

Figure 3. *In vivo* activation of BF^{Vglut2} → VTA^{Vglut2} projections suppressed food intake

(A) Schematic diagram showing strategies of virus injections and optic cannula implantations for photostimulation of BF^{Vglut2} → VTA^{Vglut2} projections.

(B) Representative expression patterns of the injected ChR2 virus and cannula tracks in the VTA. Fos is a marker of neuronal activation in mice. Scale bars, 200 μm.

(C) Quantitative comparisons of Fos-positive neuron numbers at different bregma levels (from anterior to posterior) between control EYFP and ChR2 groups. Two-way ANOVA followed by Sidak multiple comparisons test; from anterior to posterior bregma levels: $F(1, 48) = 56.18$; $p < 0.0001$.

(D) The self-comparison in food intake between laser off and 20 Hz–20 ms stimulation in both EYFP and ChR2 groups. Two-way ANOVA followed by Sidak multiple comparisons test: $F(1, 31) = 16.29$, $p = 0.0003$.

(E) The self-comparisons in food intake between laser off, 20 Hz–20 ms, 20 Hz–20 ms with DNQX/AP5 in the ChR2 group. Animals n = 5. One-way repeated ANOVA followed by Turkey multiple comparisons test: laser off vs. 20 Hz, 20 ms, $p = 0.0206$; 20 Hz, 20 ms vs. 20 Hz, 20 ms (DNQX + AP5), $p = 0.0063$.

(F) Quantitative comparisons in distance and time in the center in the open field test (OFT) between the two groups. Two-way ANOVA followed by Sidak multiple comparisons test: distance, $F(2, 26) = 20.71$, $p < 0.0001$; time in center, $F(2, 24) = 11.60$, $p = 0.0003$.

(G) Representative moving tracks (pink color) of animals from EYFP (top) and ChR2 (bottom) groups in the real-time place avoidance test. The left half of chamber (blue and light cyan color) was paired with photostimulation (20 Hz, 20 ms), whereas the right half (gray color) was not.

(legend continued on next page)

(Figures S3F, S3G, S3I, and S3J), which is in line with the notion that these neurons are directly downstream of BF glutamatergic neurons.

Activation of BF^{Vglut2} → VTA circuit reduces feeding and causes avoidance

Heightened activity of BF^{Vglut2} neurons is known to inhibit food intake.[15] Given that we revealed BF^{Vglut2} → VTA^{Vglut2} connectivity, we reasoned that VTA^{Vglut2} neurons may mediate the effects on feeding. To test this, we utilized ChR2-based *in vivo* optogenetics to activate BF^{Vglut2} neuronal fibers within the VTA (Figure 3A). Toward this, we delivered AAV5-Ef1a-DIO-ChR2-EYFP in the BF of Vglut2-Cre mice and implanted fiber optic cannulas over the VTA. Photostimulation (λ = 473 nm, 20 Hz–20 ms, 10 min) of ChR2-positive fibers within the VTA was found to significantly increase Fos in the subset of VTA neurons (Figures 3B and 3C), confirming the functional activation of these neurons. Next, in fasted mice, *in vivo* photostimulation of the BF^{Vglut2} → VTA circuit reduced food consumption and feeding duration (Figures 3D and S3L–S3N). This effect was partially rescued by the administration of glutamate receptor antagonists AP5 ((2*R*)-amino-5-phosphonovaleric acid) and dinitroquinoxaline (DNQX) into the VTA (Figure 3E), suggesting that the reduction in feeding was mediated by the activation of glutamate receptors in the VTA. Interestingly, ChR2-expressing mice also exhibited an increased physical activity level with photostimulation (Figure 3F). To test the valence associated with the observed feeding inhibition, a real-time place avoidance (RTPA) test was conducted, in which photostimulation was paired with one-half of the arena in a counterbalanced manner. Mice expressing ChR2 spent more time in the non-stimulation half, whereas EYFP-expressing controls showed no preference for either side, suggesting an avoidance behavior elicited by the activation of the BF^{Vglut2} → VTA circuit (Figures 3G–3I), which was associated with an increased velocity (Figure 3I), consistent with the increased locomotion observed in the open field test (OFT) (Figure 3F). Since VTA-projecting BF^{Vglut2} neurons also send collateral projections to the LHb and other brain regions, the observed behavioral effects may be partly mediated by these additional projection sites through parallel activations. To test this possibility, we performed the same experiment but with simultaneous inhibition of BF^{Vglut2} neuron somas, which would largely eliminate collateral activation. We expressed the inhibitory designer receptor exclusively activated by designer drugs (hM4Di) in BF^{Vglut2} neurons (Figure 3J).[49] Clozapine N-oxide (CNO) treatment effectively reduced Fos expression in BF^{Vglut2} neurons induced by activation of glutamatergic fibers in the VTA (Figures 3K and 3L), confirming an effective inhibition of BF^{Vglut2} neurons. Behaviorally, with the presence of CNO, photostimulation of BF^{Vglut2} fibers in the VTA was still able to induce aversion, increase physical activity, and reduce fasting refeeding (Figures 3M and 3N), suggesting that the observed effects were mediated by BF^{Vglut2} projections within the VTA.

Activation of VTA^{Vglut2} neurons reduces motivational feeding and body weight and increases activity

Given that VTA^{Vglut2} neurons are one of the major downstream targets of BF^{Vglut2} neurons, we next examined the role of VTA^{Vglut2} neurons in feeding regulation. Toward this, we first employed a hM3Dq-dependent chemogenetic method to activate VTA^{Vglut2} neurons in the short term and assessed the effects (Figure 4A).[49] We delivered AAV9-hSyn-DIO-hM3Dq-mCherry or AAV5-hSyn-DIO-mCherry viral particles to the VTA of Vglut2-Cre mice. Notably, the administration of the hM3Dq agonist CNO (i.p., 1 mg/kg) significantly increased Fos expression in hM3Dq-mCherry-expressing neurons compared with the mCherry group (Figures 4B and 4C). Also, CNO administration in the hM3Dq group greatly reduced fasting-induced refeeding compared with saline, whereas it had no effects in the mCherry group within 6 h after treatments (Figure 4D). Given the role of VTA^{Vglut2} neurons in reward processing,[50,51] we further explored the effects of these neurons in food motivation. For this, mice were trained through an established protocol to perform nose pokes at the correct port for sucrose pellets with increasing fixed ratios (FRs) until they reached the point of acquiring more than 20 sucrose pellets at FR = 15 within a 30-min session (Figure 4E). During the testing episode, CNO administration completely blocked nose poke behaviors for sucrose pellets in the hM3Dq group, whereas it had no effects on the mCherry control group (Figure 4F). To test the motivation for HFD, we conducted an HFD-preference test, in which 6-h fasted mice were able to freely access HFD and chow diet (CD). In the control group, we observed a high preference for HFD toward CD, which was blunted in the hM3Dq group (Figure 4G). These results demonstrated a profound effect of VTA^{Vglut2} neuron activation on suppressing motivational feeding behaviors. Consistent with the increase in physical activity by *in vivo* photostimulation of the BF^{Vglut2} → VTA circuit, CNO-mediated activation of VTA^{Vglut2} neurons increased physical activity measured in metabolic cages (Figures 4H and 4I). Since changes in feeding are known to be associated with altered anxiety,[1] we further assessed the anxiety level in these mice using the light-dark box test (LDT). Compared with saline treatments, CNO application in the hM3Dq group reduced time spent in the light side of the box, whereas CNO had no effects in the mCherry group (Figures 4J and 4K), suggesting that CNO-induced activation of VTA^{Vglut2} neurons elicited anxiety-like behavior. In sum, activation of VTA^{Vglut2} neurons

(H and I) Quantitative comparisons in duration and velocity in two halves of chambers between control EYFP and ChR2 groups. Two-way ANOVA followed by Sidak multiple comparisons test: (H) $F(1, 13) = 61.16$, $p < 0.0001$; (I) $F(1, 12) = 16.83$, $p = 0.0015$.

(J) Schematic diagram showing virus injections and optic cannula implantation to test the behavioral effects of inhibiting co-lateral projections from VTA-projecting BF^{Vglut2} neurons.

(K) Fos expression patterns in the BF of animals that received 10-min laser stimulation with or without treatment of CNO.

(L) Qualitative results of Fos expressions within the BF. Unpaired t test: $p = 0.0317$.

(M and N) Quantification results of fasting-refeeding test (M) and real-time place avoidance test (N). Two-way ANOVA followed by Sidak multiple comparisons test: (M) $F(1, 6) = 0.0008487$, $p = 0.9777$; (N) $F(1, 8) = 23.61$, $p = 0.0013$.

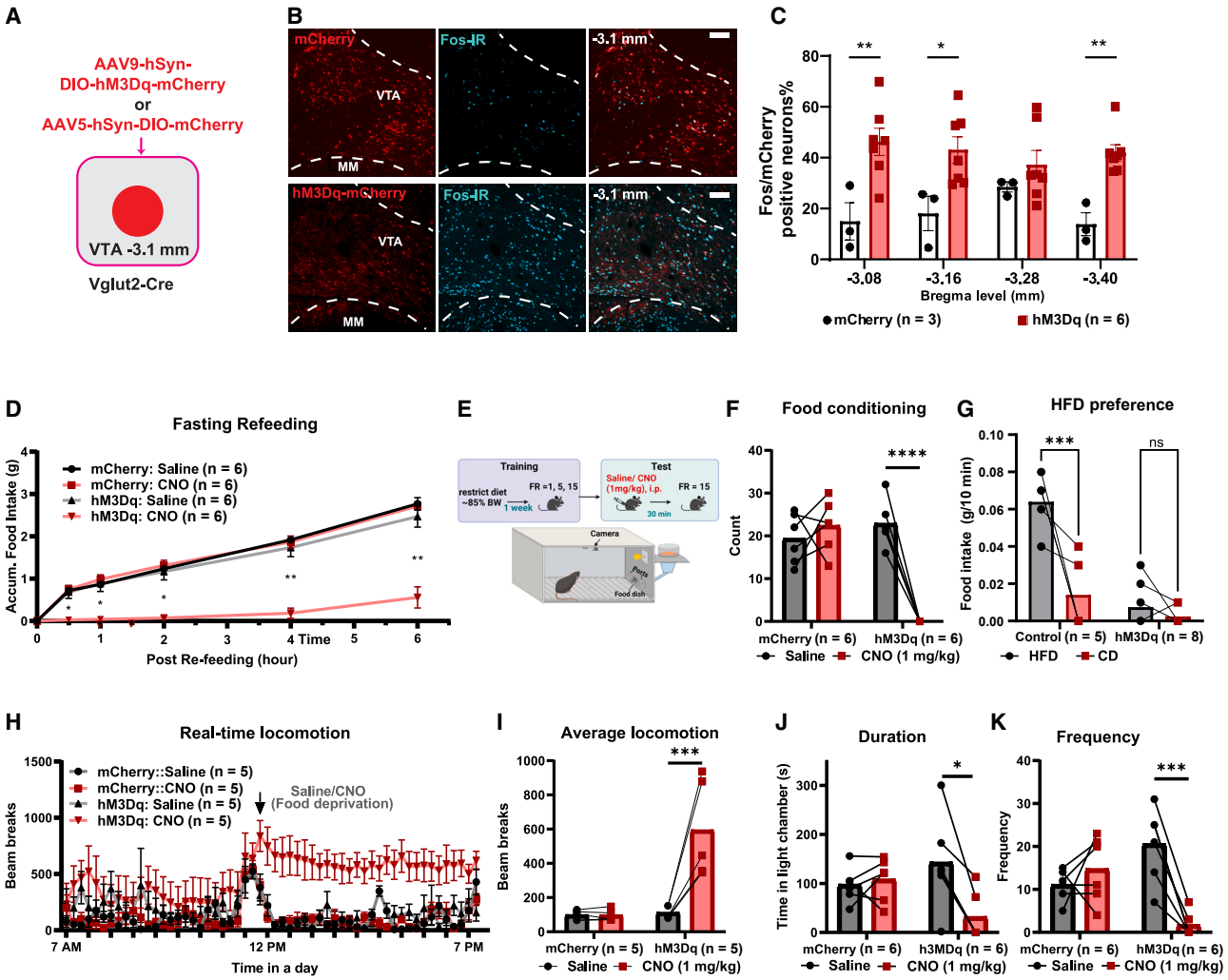

Figure 4. Acute activation of VTA^{Vglut2} neurons decreased food motivation and induces anxiety

(A) Schematic diagram showing the hM3Dq virus injection in VTA^{Vglut2} neurons for chemogenetic activation.

(B) Expression pattern of mCherry (top) or hM3Dq (bottom) and Fos immunostaining in the VTA. Scale bars, 200 μm.

(C) Qualitative comparisons in the percentages of Fos-positive neurons in the viral (mCherry)-labeled neurons shown in an anterior to posterior bregma order. Two-way repeated ANOVA followed by Sidak multiple comparisons test: $F(1, 32) = 30.24$, $p < 0.0001$.

(D) Comparisons in cumulative fasting-refeeding food intake within 6 h post saline and CNO application between mCherry and hM3Dq groups. Two-way ANOVA followed by Sidak multiple comparisons test: $F(15, 105) = 19.90$, $p < 0.0001$.

(E) Schematic diagram showing procedures and timing of nose poke training and testing in mice. FR, fixed ratio.

(F) Comparisons in sucrose pellets acquired during the testing session between the mCherry and hM3Dq groups after saline and CNO application. Two-way ANOVA followed by Sidak multiple comparisons test: $F(1, 10) = 56.42$, $p < 0.0001$.

(G) Qualitative results of HFD-preference test in control and hM3Dq groups. Two-way ANOVA followed by Sidak multiple comparisons test: $F(1, 11) = 13.18$, $p = 0.004$.

(H) Real-time locomotor activities from metabolic cages. The arrow indicates when the mice were injected with saline or CNO.

(I) Comparisons of average locomotion within 6 h after saline or CNO treatment. Two-way repeated ANOVA followed by Sidak multiple comparisons test: $F(1, 8) = 17.76$, $p = 0.0029$.

(J and K) Comparisons of time spent (J) and frequency entering (K) in light chambers during the light-dark box test. Two-way repeated ANOVA followed by Sidak multiple comparisons test: (J) $F(1, 10) = 11.41$, $p = 0.007$; (K) $F(1, 10) = 21.39$, $p = 0.0009$.

led to increased locomotion, increased anxiety-like behaviors, and hypophagia with reduced motivation for food.

Since VTA$^{Vglut2+/Vgat-}$ and VTA$^{Vglut2+/Vgat+}$ neurons are both downstream of BF glutamatergic neurons, we also examined the effect of hM3Dq activation of these neurons (Figures S3O–S3T). Although CNO-mediated activation of VTA$^{Vglut2+/Vgat-}$ neurons reduced feeding and increased locomotion (Figures S3O–S3Q), activating VTA$^{Vglut2+/Vgat+}$ neurons had no impact on feeding or locomotion (Figures S3R–S3T), suggesting a role for VTA$^{Vglut2+/Vgat-}$ neurons in mediating hypophagia and hyperactivity caused by the activation of BF glutamatergic projections.

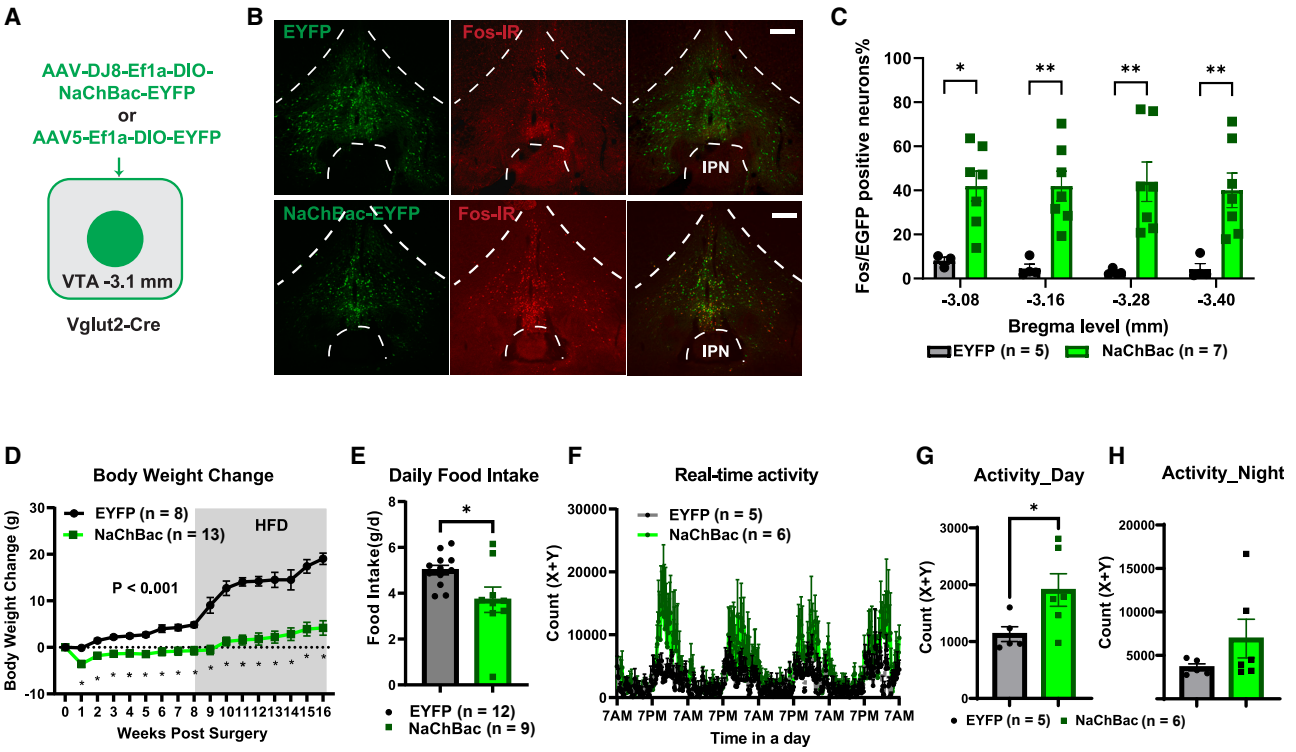

Figure 5. Effects of chronic activation of VTA^{Vglut2} neurons led to major hallmarks of anorexia

(A) Schematic diagram showing injections of the NaChBac virus to the VTA for chronic activation of VTA^{Vglut2} neurons.

(B) Representative coronal sections of the VTA showing Fos immunostaining from EYFP (top) and NaChBac (bottom) mice. Scale bars, 200 μm.

(C) Quantitative comparisons in the number of Fos-positive neurons in EGFP-labeled Vglut2 neurons between control and NaChBac mice. Two-way ANOVA followed by Sidak multiple comparisons test: F (1, 35) = 46.51, p < 0.0001.

(D) Comparisons in weekly body weight for the 16 weeks after viral delivery. From 0 to 8 weeks post-surgery, mice were fed chow diet and from 9 to 16 weeks post-surgery, mice were fed with high-fat diet (HFD). Two-way repeated ANOVA followed by Sidak multiple comparisons test: F (16, 190) = 17.22, p < 0.0001.

(E) The comparison in daily food intake on chow diet between the two groups. Unpaired Student's t test, p = 0.0251.

(F) Real-time locomotor activity patterns measured by the comprehensive laboratory animal monitoring system (CLAMS) metabolic cages.

(G and H) Comparisons in the locomotor activity levels measured during periods of the day (left) and the night (right). Unpaired t test: (G) p = 0.0475; (H) p = 0.2154.

Since anorexia symptoms are likely caused by chronic changes in neuronal activity, we next explored the effect of chronic activation of VTA^{Vglut2} neurons utilizing a mutated sodium channel from bacteria (NaChBac) that enables long-term activation.[52,53] We delivered to the VTA of Vglut2-Cre male mice with AAV-DJ8-Ef1a-DIO-NaChBac-EGFP or control AAV5-Ef1a-DIO-EYFP viral vectors (Figure 5A). Immunostaining results showed that NaChBac expression led to a dramatic increase in Fos expression in the VTA, confirming the activation of VTA^{Vglut2} neurons (Figures 5B and 5C). Interestingly, mice with NaChBac expression showed lower body weight and resistance to diet-induced obesity compared with the EYFP-injected control group (Figure 5D). Consistent with lower body weight, the NaChBac group displayed lower food intake when compared with controls (Figure 5E). When measured in metabolic cages to collect real-time physiological data, compared with controls, the NaChBac group showed increased locomotion (Figures 5F–5H), suggesting that the lower body weight was due to severe energy deficits. Of note, we observed a similar phenotype in female Vglut2-Cre mice (Figure S4). Together, these results demonstrate that chronic activation of VTA^{Vglut2} neurons causes hypophagia, decreased body weight gain, and higher locomotion.

The BF^{Vglut2} → VTA^{Vglut2} projection suppresses DA release

Changes in DA signaling have been associated with lower body weights.[54] Given the newly revealed role of the BF^{Vglut2} → VTA^{Vglut2} circuit in motivational feeding, we further investigated the potential effects of this projection in modulating DA release. The NAc is one of the major downstream regions of VTA DA neurons for reward and salience processing; hence, we recorded dynamic DA release in the NAc using gGRAB-DA3m (gDA3m)-based fiber photometry recording in freely moving mice.[55] For this, we delivered an AAV9-hSyn-gDA3m virus to the shell of NAc (NAcSh) and implanted optic fiber cannulas targeting the same region (Figures 6A and 6B). Consistent with previous results in sucrose consumption,[32,56] we detected an increase in DA release in the NAcSh when mice consumed an HFD pellet (Figures 6C–6E). In addition, we observed reduced DA release when mice received an aversive stimulus such as water spray (Figures S5A–S5C). Interestingly, we

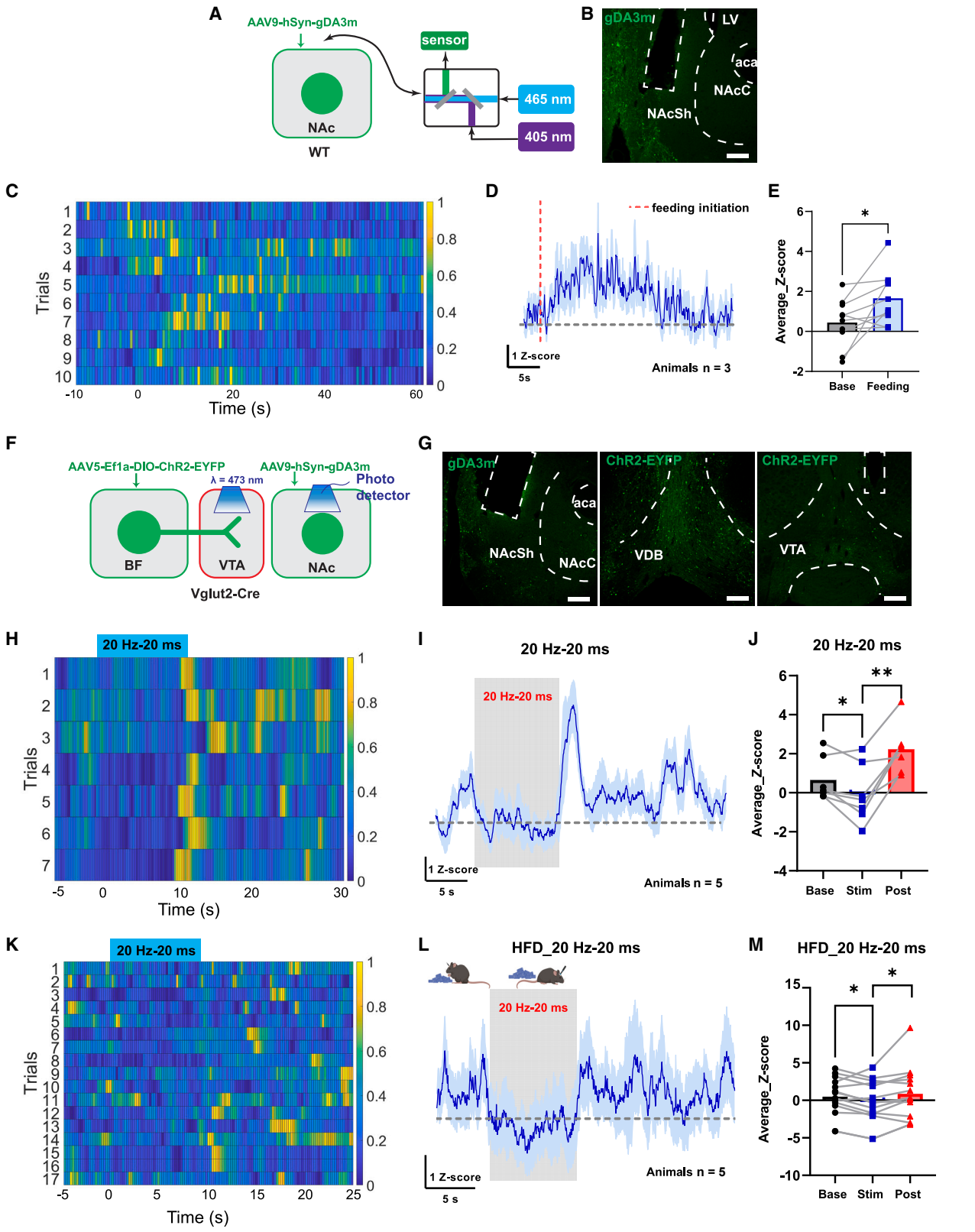

(legend on next page)

observed a rebound in DA release following the suppression period induced by aversive stimuli (Figures S5A–S5C), reminiscent of the comforting effect of the "pain relief" observed previously.[57]

Finally, to examine the effect of $BF^{Vglut2} \rightarrow VTA^{Vglut2}$ projections on DA release, we recorded DA release while activating BF^{Vglut2} fibers in the VTA via targeted photostimulation (Figure 6F). Toward this, we delivered AAV5-Ef1a-DIO-ChR2-EYFP in the BF of Vglut2-Cre mice and implanted optic cannulas in the VTA in addition to delivering gDA3m virus and implanted optic fibers in the NAcSh (Figure 6G). Photostimulations of the BF → VTA circuit with laser at 20 Hz–20 ms for 10 and 20 s both reduced DA release in a duration-dependent manner (Figures 6H–6J and S5D–S5F). To explore the relationship between DA release regulated by $BF^{Vglut2} \rightarrow VTA^{Vglut2}$ projections and feeding behaviors, we monitored DA release in response to photostimulation when mice initiated HFD feeding bouts. In this regard, *ad libitum* mice were allowed to move freely to reach an HFD pellet placed in one corner of the cage. At the time when the mice started consuming pellets, photostimulation was applied to activate the $BF^{Vglut2} \rightarrow VTA^{Vglut2}$ projection for 10 s (Figures 6K–6M). The signals for DA release increased when mice were involved in pellet consumption and were reduced upon photostimulation, which was also associated with an immediate pause in feeding and a roam away from the food (Figure 6L). These results collectively suggest that activation of $BF^{Vglut2} \rightarrow VTA^{Vglut2}$ projection reduces feeding and involves reduced DA release in the NAc.

VTA^{Vglut2} neurons are known to project to GABAergic neurons in the NAc,[58] which have been shown to be able to reduce VTA DA neuron activity.[59] Consistently, we observed projection fibers in the NAc from VTA^{Vglut2} neurons that received projections from BF^{Vglut2} neurons (Figures S5G and S5H). In addition, we noticed that there was an increase in Fos expression in the NAc following photostimulating BF to VTA glutamatergic terminals at the VTA (Figures S5I–S5L). This set of data supports a potential role for $VTA^{Vglut2+/Vgat-}$ neurons in mediating the change in DA release.

DISCUSSION

An appropriate decision to engage in feeding is an adaptive behavior that integrates perceived stress and internal energy needs. Environmental disturbances cause stress and limit feeding, even when mice have great energy demands. Several studies on stress-induced hypophagia have focused on neural pathways that process sensory cues for threats, which also elicit behavioral signs of stress and inhibit feeding.[1,2] In this study, we have identified a $BF^{Vglut2} \rightarrow VTA^{Vglut2}$ circuit that is sensitive to and activated by environmental cues and is associated with reduced DA release in the NAc. *In vivo* activation of this circuit reduced feeding, increased physical activity, and caused avoidance behaviors. Similarly, activation of downstream VTA^{Vglut2} neurons diminished food motivation, caused hyperactivity, and increased behavioral signs of anxiety. Consistently, mice with chronic activation of VTA^{Vglut2} neurons exhibited hypophagia and reduced body weight associated with heightened physical activity. Interestingly, the observed phenotypes represent typical behavioral and physiological signs observed in patients with anorexia nervosa, the core symptoms of which include voluntary starvation, hyperactivity, and anxiety.[5,6,60] Our extensive functional-tracing experiments further identified $VTA^{Vglut2+/Vgat-}$ and $VTA^{Vglut2+/Vgat+}$ neurons as the major downstream VTA neurons mediating the effect. Taken together, our results reveal that overactivation of the $BF^{Vglut2} \rightarrow VTA^{Vglut2}$ circuit may contribute to the pathogenesis of anorexia.

Consistent with previous observations that BF neurons respond to volatile odors and predator cues,[15,17,18] here, we showed that BF^{Vglut2} neurons were sensitive to various physical stressors and aversive stimuli. To extend these findings, we also found that VTA^{Vglut2} neurons are directly downstream targets of BF^{Vglut2} neurons, and they respond in a similar manner to these aversive stimuli, suggesting that they are important downstream mediators in aversive sensory perception. Our previous results showed that chronic activation of BF^{Vglut2} neurons elicited a starvation phenotype,[15] which supports our current observations that activation of the $BF^{Vglut2} \rightarrow VTA^{Vglut2}$ circuitry causes

Figure 6. DA signals decreased in the NAc in response to activation of the $BF^{Vglut2} \rightarrow VTA^{Vglut2}$ projections

(A) Schematic diagram showing virus injections and optic cannula implantations for recording DA release in the NAc.

(B) Representative coronal sections of the VTA showing gDA3m expression pattern and cannula tracks. Scale bars, 200 μm.

(C) Heatmap of DA release *Z* score signals corresponding to first feeding bouts of individual trials. Signals were re-scaled from 0 to 1 across each row.

(D) Averaged *Z* score signals of DA release in the NAc corresponding to first feeding bouts. The light blue shade represents signals with mean ± SEM. Time = 0 was the onset of feeding.

(E) Averaged *Z* scores during baseline and feeding. Paired Student's t test: p = 0.0268. Animals n = 3.

(F) Schematic diagram showing virus injections and optic cannula implantations to record DA release in the NAc with photostimulation of $BF^{Vglut2} \rightarrow VTA^{Vglut2}$ projections.

(G) Representative coronal sections of the BF, the VTA, and the NAc showing injection patterns of ChR2 and gDA3m and cannula tracks. Scale bars, 200 μm.

(H) Heatmap of DA release *Z* score signals of individual trials in response to10-s photostimulation. Signals were re-scaled from 0 to 1 across each row. The indigo box indicates the period of photostimulation.

(I) Averaged trace of DA release *Z* score signals in the NAc in response to a period of 10 s of 20 Hz–20 ms photostimulation.

(J) Averaged *Z* scores during baseline, 20 Hz–20 ms stimulation, and 5 s post-stimulation. Paired Student's t test: stim vs. base, p = 0.0349; post vs. stim, p = 0.0019. Animals n = 5.

(K) Heatmap of DA release *Z* scores signals of individual trials when mice were engaging HFD feeding with photostimulation. Signals were re-scaled from 0 to 1 across each row. The indigo box shows the period with photostimulation.

(L) Averaged signals of DA release in the NAc in response to a period of 10 s of 20 Hz–20 ms photostimulation right after the onset of HFD feeding. The blue shade represents signals in ±SEM. Time = 0 was the onset of photostimulation.

(M) Averaged *Z* scores during baseline, 20 Hz–20 ms photostimulation, and 5 s post-stimulation. Paired Student's t test: stim vs. base, p = 0.0213; post vs. stim, p = 0.0223. Base, baseline; stim, 20 Hz–20 ms photostimulation; post, 5 s post-photostimulation. Animals n = 5.

anorexia-like behaviors. Taken together, these observations support that BF^{Vglut2} neurons function as a primary node in the brain that senses external threat cues and overrides energy needs to avoid potential risks. Since VTA is known to be involved in motivation and feeding, the $BF^{Vglut2} \rightarrow VTA^{Vglut2}$ circuit is well-positioned to integrate sensory cues and impact motivational feeding behaviors. It is worth noting that the VTA-projecting BF^{Vglut2} neurons also send collaterals to other brain regions, including LHb and LH neurons. Previous studies suggest that both LH and LHb neurons mediate the action of BF^{Vglut2} neurons in feeding inhibition.[15,17] Since both the LH and LHb have been shown to project to the VTA,[61,62] the VTA represents a convergent brain target from various brain sites in mediating adaptive feeding behaviors to ongoing environmental threat cues. Related to this point, we did not observe an effect on feeding or body weight at the *ad libitum* condition when we disrupted glutamatergic signaling from VTA^{Vglut2} neurons that project to the BF (Figure S6),[63] suggesting that the $BF^{Vglut2} \rightarrow VTA^{Vglut2}$ circuit is not required for normal feeding regulation. This observation implies that neurocircuits involved in regulating hypophagia, i.e., in anorexia, can be dissociated with those in hyperphagia, i.e., obesity development.

Despite extensive studies on the pathogenesis of anorexia, the underlying brain mechanism remains elusive. One of the major difficulties in this line of research lies in the lack of reliable animal models that could closely capture the symptoms observed in human patients with anorexia nervosa.[64] Previous studies involving brain-derived neurotrophic factor or activity-based anorexia all involve forced feeding restriction,[64,65] which is opposite to voluntary feeding restriction observed in human patients. Regarding this, chronic activation of BF^{Vglut2} neurons has been shown to cause a voluntary starvation phenotype.[15] Consistently, our current results demonstrate that chronic activation of VTA^{Vglut2} neurons, as one of the downstream targets of BF^{Vglut2} neurons, led to voluntary starvation associated with reduced motivation for feeding, heightened locomotion, and diminished HFD-induced obesity. These observations, taken together, support the idea that uncontrolled overactivation of the $BF^{Vglut2} \rightarrow VTA^{Vglut2}$ circuit may contribute to anorexia-like phenotypes. Given the role of BF^{Vglut2} neurons in sensing environmental cues,[15] it is conceivable that hypersensitivity by these neurons to environmental threats may cause overactivation. Given their function in memory and conditioning,[7,66] activation of BF neurons may also be caused by various conditioned cues, which may also lead to a predisposition to the development of anorexia. In particular, chemogenetic activation of VTA^{Vglut2} neurons caused anxiety-like behaviors, which is in line with previous studies showing that sustained stimulation of VTA^{Vglut2} neurons is less preferred and causes behavioral avoidance.[35,58] Previous studies also suggest a role of VTA^{Vglut2} neurons in driving arousal, exploration, and facilitating defensive escape behaviors, which are all associated with hyperactivity, supporting a role for these neurons in increasing locomotion.[44,67] In addition, glutamatergic action in the NAc has been shown to increase locomotion.[68,69] These results, combined with our results on $VTA^{Vglut2+/Vgat-}$ neurons in mediating feeding/activity, support that $VTA^{Vglut2+/Vgat-}$ neurons play a main role in mediating the action of glutamatergic BF to VTA projections in promoting anorexia-like symptoms.

It is not clear whether and to what extent the observed reduction in DA release contributes to the hypophagia phenotype. It was previously shown that modulation of DA receptor D2 (DRD2) signaling in the NAc caused anorexia-like behaviors in mice.[70] In addition, changes in DA signaling were observed in patients diagnosed with anorexia nervosa.[54,71] Human studies suggest a negative correlation between DRD2 levels and BMI.[72] Animal studies suggest that an increase in DA signals is generally associated with positive valence and reward or reward-related cues,[32,56,73,74] whereas complete loss of DA release leads to a lethal phenotype, which can be rescued by the recovery of feeding through increasing DA release in the striatum.[75] These observations support the possibility that the hypophagia caused by overactivation of the $BF^{Vglut2} \rightarrow VTA^{Vglut2}$ circuit is mediated by reduction in DA release in the striatum.

It is well known that anorexia occurs at a much higher rate in women than in men.[76] However, current data suggest that female mice exhibited a similar spectrum of anorexia-like phenotypes to males, suggesting that there is no sexual dimorphism regarding the BF glutamatergic projection to VTA in producing anorexia-like phenotypes. Since men are also known to develop anorexia, albeit at a much lower frequency, the BF → VTA glutamatergic pathway may represent a common pathway between males and females that regulates stress-related hypophagia.

In summary, our results presented here support the conclusion that the $BF^{Vglu2} \rightarrow VTA^{Vglut2}$ circuit functions to sense environmental threats and adjust adaptive behaviors in feeding during hunger-threat conflict situations. Overactivation of this circuit led to hypophagia, reduced motivation for feeding, hyperactivity, and anxiety-like behaviors, all typical signs of anorexia. In addition to glutamatergic neurons, the BF also contains GABAergic and cholinergic neurons, both of which are also sensitive to environmental cues for threats,[9–11] suggesting a general role for the BF in surveying external cues and mediating necessary adaptation for survival. Since BF^{Vglut2} neurons send projections to several brain sites that also reduce feeding, VTA^{Vglut2} neurons may represent one downstream neuronal population that mediates the adaptive behaviors elicited by cue-activated BF^{Vglut2} neurons.[15,17] Since VTA^{Vglut2} neurons have also been shown to receive multiple upstream inputs implicated in mediating behaviors that include sleep, defense, and exercise,[28,51] in addition to feeding behaviors shown here, VTA^{Vglut2} neurons appear to serve as a hub, integrating both external and internal cues to mediate adaptive feeding behaviors toward the ever-changing environment.

Limitations of the study

It is somewhat surprising that the observed increased activity is associated with reduced DA release. However, although increased DA release is known to promote locomotion,[77] changes in locomotion may not always be correlated with changes in DA release. For example, during HFD consumption, DA release in the NAc is known to be increased[32,56] (also see Figure 6), but without an increase in activity. Notably, a similar observation was also observed in previous studies on

glutamatergic LH projections to VTA, in which photostimulation was shown to reduce DA release in NAc[78] and also cause defensive escaping,[44] a behavior associated with increased locomotion.

Since the current focus is on the BF to VTA projection, our current data could not provide a definitive answer to the underlying mechanism for the reduced DA release, i.e., it is unknown whether the reduced DA release is related to hypophagia, reduced activity, both, or neither. A challenge to delineate the exact mechanism underlying the reduced DA release lies in the functional complexity of VTA subsets of neurons. For example, VTA GABAergic neurons have been shown to support reward or disrupt reward/promote aversion.[31,33,59,79] VTA glutamatergic neurons have also been shown to cause place aversion or preference.[34,35] Specifically, despite the literature on VTA^{Vglut2} neurons in causing aversion that is consistent with our findings, other studies suggest that direct optical activation of VTA^{Vglut2} neurons can induce appetitive operant conditioning and reinforcement in the absence of DA release.[34,37,80] These observations collectively suggest a functional diversity of VTA neurons. Previous studies suggest that within VTA^{Vglut2} neurons, $VTA^{Vglut2+/Vgat-}$ neurons project to the NAc, whereas $VTA^{Vglut2+/Vgat+}$ neurons project to the LHb.[45] Importantly, VTA^{Vglut2} neurons project to GABAergic neurons in the NAc,[58] which has been shown to be able to reduce VTA DA neuron activity.[59] Under this context, we noticed that there was an increase in Fos expression in the Nac following photostimulating glutamatergic BF to VTA terminals in the VTA, supporting a potential contribution of $VTA^{Vglut2+/Vgat-}$ neurons to the observed reduced DA release. However, among many other possibilities, $VTA^{Vglut2+/Vgat+}$ neurons, which, although not important in mediating feeding or activity, may separately mediate the effect on reducing DA through projecting to the LHb, which has been demonstrated to be able to reduce VTA DA neuron activity through excitatory projections to rostromedial tegmental nucleus GABA neurons.[81–83] Given the complexity of VTA local and remote circuits, further studies are required to understand the diverse and, sometimes, contrasting roles of VTA neurons.

STAR★METHODS

Detailed methods are provided in the online version of this paper and include the following:

- KEY RESOURCES TABLE
- RESOURCE AVAILABILITY
  - Lead contact
  - Materials availability
  - Data and code availability
- EXPERIMENTAL MODEL AND STUDY SUBJECT DETAILS
- METHOD DETAILS
  - Stereotaxic surgery
  - Brain slice electrophysiological recordings
  - Fiber photometry
  - *In vivo* photostimulation
  - Real-time place avoidance (RTPA)
  - Fasting refeeding assay
  - Laser on-off open field test
  - Chemogenetics
  - Singly housed fasting refeeding assay
  - Operant conditioning
  - HFD preference test
  - LDT and OFT
  - Physiology assessment
  - Post-hoc analysis
- QUANTIFICATION AND STATISTICAL ANALYSIS

SUPPLEMENTAL INFORMATION

Supplemental information can be found online at https://doi.org/10.1016/j.neuron.2023.11.001.

ACKNOWLEDGMENTS

We acknowledge Dr. Yulong Li for providing the gDA3m vector. This study was supported by the NIH R01 DK135212, R01DK131446, and R01DK136284 (Q.T.); R01 DK120858 (Q.T. and Yong Xu); R01DK109934 and DOD HT94252310156 (Q.T. and B.R.A.). Q.T. is the holder of the Cullen Chair in Molecular Medicine at McGovern Medical School. J.C. is the awardee of the Russell and Diana Hawkins Family Foundation Discovery Fellowship. The figure abstract and some diagrams were created with BioRender.com.

AUTHOR CONTRIBUTIONS

J.C. conducted the major part of research with help from Y.J., Yuanzhong Xu, and Z.J. Y.J. conducted the brain-slice recordings. J.O.-G., B.R.A., Yong Xu, Y.Z., and Y.L. provided essential reagents. Q.T. and B.R.A. conceived and designed the experiments and wrote the manuscript with significant inputs from all authors.

DECLARATION OF INTERESTS

The authors declare no competing interests.

INCLUSION AND DIVERSITY

We support inclusive, diverse, and equitable conduct of research.

Received: May 10, 2023
Revised: October 4, 2023
Accepted: November 3, 2023
Published: December 5, 2023

REFERENCES

1. Maniscalco, J.W., and Rinaman, L. (2017). Interoceptive modulation of neuroendocrine, emotional, and hypophagic responses to stress. Physiol. Behav. *176*, 195–206.
2. Francois, M., Canal Delgado, I., Shargorodsky, N., Leu, C.S., and Zeltser, L. (2022). Assessing the effects of stress on feeding behaviors in laboratory mice. eLife *11*, e70271.
3. Torres, S.J., and Nowson, C.A. (2007). Relationship between stress, eating behavior, and obesity. Nutrition *23*, 887–894.
4. Nakamura, C., Ishii, A., Matsuo, T., Ishida, R., Yamaguchi, T., Takada, K., Uji, M., and Yoshikawa, T. (2020). Neural effects of acute stress on appetite: A magnetoencephalography study. PLoS One *15*, e0228039.
5. Thornton, L.M., Dellava, J.E., Root, T.L., Lichtenstein, P., and Bulik, C.M. (2011). Anorexia nervosa and generalized anxiety disorder: further explorations of the relation between anxiety and body mass index. J. Anxiety Disord. *25*, 727–730.
6. Dellava, J.E., Kendler, K.S., and Neale, M.C. (2011). Generalized anxiety disorder and anorexia nervosa: evidence of shared genetic variation. Depress. Anxiety *28*, 728–733.

7. Blake, M.G., and Boccia, M.M. (2018). Basal forebrain cholinergic system and memory. Curr. Top. Behav. Neurosci. *37*, 253–273.

8. Xu, M., Chung, S., Zhang, S., Zhong, P., Ma, C., Chang, W.-C., Weissbourd, B., Sakai, N., Luo, L., and Nishino, S. (2015). Basal forebrain circuit for sleep-wake control. Nat. Neurosci. *18*, 1641–1647.

9. Goard, M., and Dan, Y. (2009). Basal forebrain activation enhances cortical coding of natural scenes. Nat. Neurosci. *12*, 1444–1449.

10. Pinto, L., Goard, M.J., Estandian, D., Xu, M., Kwan, A.C., Lee, S.H., Harrison, T.C., Feng, G., and Dan, Y. (2013). Fast modulation of visual perception by basal forebrain cholinergic neurons. Nat. Neurosci. *16*, 1857–1863.

11. Rothermel, M., Carey, R.M., Puche, A., Shipley, M.T., and Wachowiak, M. (2014). Cholinergic inputs from basal forebrain add an excitatory bias to odor coding in the olfactory bulb. J. Neurosci. *34*, 4654–4664.

12. Zhu, F., Elnozahy, S., Lawlor, J., and Kuchibhotla, K.V. (2023). The cholinergic basal forebrain provides a parallel channel for state-dependent sensory signaling to auditory cortex. Nat. Neurosci. *26*, 810–819.

13. Romanov, R.A., Zeisel, A., Bakker, J., Girach, F., Hellysaz, A., Tomer, R., Alpár, A., Mulder, J., Clotman, F., Keimpema, E., et al. (2017). Molecular interrogation of hypothalamic organization reveals distinct dopamine neuronal subtypes. Nat. Neurosci. *20*, 176–188.

14. Zhu, C., Yao, Y., Xiong, Y., Cheng, M., Chen, J., Zhao, R., Liao, F., Shi, R., and Song, S. (2017). Somatostatin neurons in the basal forebrain promote high-calorie food intake. Cell Rep. *20*, 112–123.

15. Patel, J.M., Swanson, J., Ung, K., Herman, A., Hanson, E., Ortiz-Guzman, J., Selever, J., Tong, Q., and Arenkiel, B.R. (2019). Sensory perception drives food avoidance through excitatory basal forebrain circuits. eLife *8*, e44548.

16. Herman, A.M., Ortiz-Guzman, J., Kochukov, M., Herman, I., Quast, K.B., Patel, J.M., Tepe, B., Carlson, J.C., Ung, K., Selever, J., et al. (2016). A cholinergic basal forebrain feeding circuit modulates appetite suppression. Nature *538*, 253–256.

17. Swanson, J.L., Ortiz-Guzman, J., Srivastava, S., Chin, P.-S., Dooling, S.W., Hanson Moss, E., Kochukov, M.Y., Hunt, P.J., Patel, J.M., Pekarek, B.T., et al. (2022). Activation of basal forebrain-to-lateral habenula circuitry drives reflexive aversion and suppresses feeding behavior. Sci. Rep. *12*, 22044.

18. Cai, P., Chen, H.Y., Tang, W.T., Hu, Y.D., Chen, S.Y., Lu, J.S., Lin, Z.H., Huang, S.N., Hu, L.H., Su, W.K., et al. (2022). A glutamatergic basal forebrain to midbrain circuit mediates wakefulness and defensive behavior. Neuropharmacology *208*, 108979.

19. Arias-Carrión, O., Stamelou, M., Murillo-Rodríguez, E., Menéndez-González, M., and Pöppel, E. (2010). Dopaminergic reward system: a short integrative review. Int. Arch. Med. *3*, 24.

20. Shohamy, D., and Adcock, R.A. (2010). Dopamine and adaptive memory. Trends Cogn. Sci. *14*, 464–472.

21. Schultz, W. (2013). Updating dopamine reward signals. Curr. Opin. Neurobiol. *23*, 229–238.

22. Vucetic, Z., and Reyes, T.M. (2010). Central dopaminergic circuitry controlling food intake and reward: implications for the regulation of obesity. Wiley Interdiscip. Rev. Syst. Biol. Med. *2*, 577–593.

23. Dietrich, M.O., Bober, J., Ferreira, J.G., Tellez, L.A., Mineur, Y.S., Souza, D.O., Gao, X.-B., Picciotto, M.R., Araújo, I., Liu, Z.-W., and Horvath, T.L. (2012). AgRP neurons regulate development of dopamine neuronal plasticity and nonfood-associated behaviors. Nat. Neurosci. *15*, 1108–1110.

24. Mazzone, C.M., Liang-Guallpa, J., Li, C., Wolcott, N.S., Boone, M.H., Southern, M., Kobzar, N.P., Salgado, I.A., Reddy, D.M., Sun, F., et al. (2020). High-fat food biases hypothalamic and mesolimbic expression of consummatory drives. Nat. Neurosci. *23*, 1253–1266.

25. Perelló, M., and Zigman, J.M. (2012). The role of ghrelin in reward-based eating. Biol. Psychiatry *72*, 347–353.

26. Miletta, M.C., Iyilikci, O., Shanabrough, M., Šestan-Peša, M., Cammisa, A., Zeiss, C.J., Dietrich, M.O., and Horvath, T.L. (2020). AgRP neurons control compulsive exercise and survival in an activity-based anorexia model. Nat. Metab. *2*, 1204–1211.

27. Stutz, B., Waterson, M.J., Šestan-Peša, M., Dietrich, M.O., Škarica, M., Sestan, N., Racz, B., Magyar, A., Sotonyi, P., Liu, Z.W., et al. (2022). AgRP neurons control structure and function of the medial prefrontal cortex. Mol. Psychiatry *27*, 3951–3960.

28. Hnasko, T.S., Hjelmstad, G.O., Fields, H.L., and Edwards, R.H. (2012). Ventral tegmental area glutamate neurons: electrophysiological properties and projections. J. Neurosci. *32*, 15076–15085.

29. Morales, M., and Margolis, E.B. (2017). Ventral tegmental area: cellular heterogeneity, connectivity and behaviour. Nat. Rev. Neurosci. *18*, 73–85.

30. Dobi, A., Margolis, E.B., Wang, H.L., Harvey, B.K., and Morales, M. (2010). Glutamatergic and Nonglutamatergic neurons of the ventral tegmental area establish local synaptic contacts with dopaminergic and nondopaminergic neurons. J. Neurosci. *30*, 218–229.

31. Tan, K.R., Yvon, C., Turiault, M., Mirzabekov, J.J., Doehner, J., Labouèbe, G., Deisseroth, K., Tye, K.M., and Lüscher, C. (2012). GABA neurons of the VTA drive conditioned place aversion. Neuron *73*, 1173–1183.

32. Patriarchi, T., Cho, J.R., Merten, K., Howe, M.W., Marley, A., Xiong, W.H., Folk, R.W., Broussard, G.J., Liang, R., Jang, M.J., et al. (2018). Ultrafast neuronal imaging of dopamine dynamics with designed genetically encoded sensors. Science *360*, eaat4422.

33. van Zessen, R., Phillips, J.L., Budygin, E.A., and Stuber, G.D. (2012). Activation of VTA GABA neurons disrupts reward consumption. Neuron *73*, 1184–1194.

34. Wang, H.L., Qi, J., Zhang, S., Wang, H., and Morales, M. (2015). Rewarding effects of optical stimulation of ventral tegmental area glutamatergic neurons. J. Neurosci. *35*, 15948–15954.

35. Root, D.H., Mejias-Aponte, C.A., Qi, J., and Morales, M. (2014). Role of glutamatergic projections from ventral tegmental area to lateral habenula in aversive conditioning. J. Neurosci. *34*, 13906–13910.

36. McGovern, D.J., Polter, A.M., and Root, D.H. (2021). Neurochemical signaling of reward and aversion to ventral tegmental area glutamate neurons. J. Neurosci. *41*, 5471–5486.

37. Zell, V., Steinkellner, T., Hollon, N.G., Warlow, S.M., Souter, E., Faget, L., Hunker, A.C., Jin, X., Zweifel, L.S., and Hnasko, T.S. (2020). VTA glutamate neuron activity drives positive reinforcement absent dopamine co-release. Neuron *107*, 864–873.e4.

38. Nagel, G., Szellas, T., Huhn, W., Kateriya, S., Adeishvili, N., Berthold, P., Ollig, D., Hegemann, P., and Bamberg, E. (2003). Channelrhodopsin-2, a directly light-gated cation-selective membrane channel. Proc. Natl. Acad. Sci. USA *100*, 13940–13945.

39. Vong, L., Ye, C., Yang, Z., Choi, B., Chua, S., Jr., and Lowell, B.B. (2011). Leptin action on GABAergic neurons prevents obesity and reduces inhibitory tone to POMC neurons. Neuron *71*, 142–154.

40. Fenno, L.E., Mattis, J., Ramakrishnan, C., Hyun, M., Lee, S.Y., He, M., Tucciarone, J., Selimbeyoglu, A., Berndt, A., Grosenick, L., et al. (2014). Targeting cells with single vectors using multiple-feature boolean logic. Nat. Methods *11*, 763–772.

41. Levy, S.L., White, J.J., Lackey, E.P., Schwartz, L., and Sillitoe, R.V. (2017). WGA-Alexa conjugates for axonal tracing. Curr. Protoc. Neurosci. *79*, 1.28.21–21.28.24.

42. Tang, J.C., Drokhlyansky, E., Etemad, B., Rudolph, S., Guo, B., Wang, S., Ellis, E.G., Li, J.Z., and Cepko, C.L. (2016). Detection and manipulation of live antigen-expressing cells using conditionally stable nanobodies. eLife *5*, e15312.

43. Reinert, J.K., Sonntag, I., Sonntag, H., Sprengel, R., Pelzer, P., Lessle, S., Kaiser, M., and Kuner, T. (2019). retroLEAP: rAAV-based retrograde transsynaptic labeling, expression and perturbation. https://doi.org/10.1101/537928.

44. Barbano, M.F., Wang, H.-L., Zhang, S., Miranda-Barrientos, J., Estrin, D.J., Figueroa-González, A., Liu, B., Barker, D.J., and Morales, M. (2020). VTA glutamatergic neurons mediate innate defensive behaviors. Neuron *107*, 368–382.e8.

45. Root, D.H., Barker, D.J., Estrin, D.J., Miranda-Barrientos, J.A., Liu, B., Zhang, S., Wang, H.L., Vautier, F., Ramakrishnan, C., Kim, Y.S., et al. (2020). Distinct signaling by ventral tegmental area glutamate, GABA, and combinatorial glutamate-GABA neurons in motivated behavior. Cell Rep. *32*, 108094.

46. Chen, T.W., Wardill, T.J., Sun, Y., Pulver, S.R., Renninger, S.L., Baohan, A., Schreiter, E.R., Kerr, R.A., Orger, M.B., Jayaraman, V., et al. (2013). Ultrasensitive fluorescent proteins for imaging neuronal activity. Nature *499*, 295–300.

47. Fenno, L.E., Ramakrishnan, C., Kim, Y.S., Evans, K.E., Lo, M., Vesuna, S., Inoue, M., Cheung, K.Y.M., Yuen, E., Pichamoorthy, N., et al. (2020). Comprehensive dual- and triple-feature intersectional single-vector delivery of diverse functional payloads to cells of behaving mammals. Neuron *107*, 836–853.e11.

48. Klapoetke, N.C., Murata, Y., Kim, S.S., Pulver, S.R., Birdsey-Benson, A., Cho, Y.K., Morimoto, T.K., Chuong, A.S., Carpenter, E.J., Tian, Z., et al. (2014). Independent optical excitation of distinct neural populations. Nat. Methods *11*, 338–346.

49. Krashes, M.J., Shah, B.P., Koda, S., and Lowell, B.B. (2013). Rapid versus delayed stimulation of feeding by the endogenously released AgRP neuron mediators GABA, NPY, and AgRP. Cell Metab. *18*, 588–595.

50. Yamaguchi, T., Qi, J., Wang, H.-L., Zhang, S., and Morales, M. (2015). Glutamatergic and dopaminergic neurons in the mouse ventral tegmental area. Eur. J. Neurosci. *41*, 760–772.

51. Cai, J., and Tong, Q. (2022). Anatomy and function of ventral tegmental area glutamate neurons. Front. Neural Circuits *16*, 867053.

52. Zhu, C., Jiang, Z., Xu, Y., Cai, Z.L., Jiang, Q., Xu, Y., Xue, M., Arenkiel, B.R., Wu, Q., Shu, G., et al. (2020). Profound and redundant functions of arcuate neurons in obesity development. Nat. Metab. *2*, 763–774.

53. Li, H., Xu, Y., Jiang, Y., Jiang, Z., Otiz-Guzman, J., Morrill, J.C., Cai, J., Mao, Z., Xu, Y., Arenkiel, B.R., et al. (2023). The melanocortin action is biased toward protection from weight loss in mice. Nat. Commun. *14*, 2200.

54. Kontis, D., and Theochari, E. (2012). Dopamine in anorexia nervosa: a systematic review. Behav. Pharmacol. *23*, 496–515.

55. Zhuo, Y., Luo, B., Yi, X., Dong, H., Wan, J., Cai, R., Williams, J.T., Qian, T., Campbell, M.G., Miao, X., et al. (2023). Improved dual-color GRAB sensors for monitoring dopaminergic activity *in vivo*. https://doi.org/10.1101/2023.08.24.554559.

56. Yuan, L., Dou, Y.N., and Sun, Y.G. (2019). Topography of reward and aversion encoding in the mesolimbic dopaminergic system. J. Neurosci. *39*, 6472–6481.

57. Navratilova, E., Atcherley, C.W., and Porreca, F. (2015). Brain circuits encoding reward from pain relief. Trends Neurosci. *38*, 741–750.

58. Qi, J., Zhang, S., Wang, H.L., Barker, D.J., Miranda-Barrientos, J., and Morales, M. (2016). VTA glutamatergic inputs to nucleus accumbens drive aversion by acting on GABAergic interneurons. Nat. Neurosci. *19*, 725–733.

59. Bocklisch, C., Pascoli, V., Wong, J.C., House, D.R., Yvon, C., de Roo, M., Tan, K.R., and Lüscher, C. (2013). Cocaine disinhibits dopamine neurons by potentiation of GABA transmission in the ventral tegmental area. Science *341*, 1521–1525.

60. Raney, T.J., Thornton, L.M., Berrettini, W., Brandt, H., Crawford, S., Fichter, M.M., Halmi, K.A., Johnson, C., Kaplan, A.S., LaVia, M., et al. (2008). Influence of overanxious disorder of childhood on the expression of anorexia nervosa. Int. J. Eat. Disord. *41*, 326–332.

61. Poller, W.C., Madai, V.I., Bernard, R., Laube, G., and Veh, R.W. (2013). A glutamatergic projection from the lateral hypothalamus targets VTA-projecting neurons in the lateral habenula of the rat. Brain Res. *1507*, 45–60.

62. Omelchenko, N., Bell, R., and Sesack, S.R. (2009). Lateral habenula projections to dopamine and GABA neurons in the rat ventral tegmental area. Eur. J. Neurosci. *30*, 1239–1250.

63. Hunker, A.C., Soden, M.E., Krayushkina, D., Heymann, G., Awatramani, R., and Zweifel, L.S. (2020). Conditional single vector CRISPR/SaCas9 viruses for efficient mutagenesis in the adult mouse nervous system. Cell Rep. *30*, 4303–4316.e6.

64. Schalla, M.A., and Stengel, A. (2019). Activity based anorexia as an animal model for anorexia nervosa–A systematic review. Front. Nutr. *6*, 69.

65. Madra, M., and Zeltser, L.M. (2016). BDNF-Val66Met variant and adolescent stress interact to promote susceptibility to anorexic behavior in mice. Transl. Psychiatry *6*, e776.

66. Harrison, T.C., Pinto, L., Brock, J.R., and Dan, Y. (2016). Calcium imaging of basal forebrain activity during innate and learned behaviors. Front. Neural Circuits *10*, 36.

67. Yu, X., Li, W., Ma, Y., Tossell, K., Harris, J.J., Harding, E.C., Ba, W., Miracca, G., Wang, D., Li, L., et al. (2019). GABA and glutamate neurons in the VTA regulate sleep and wakefulness. Nat. Neurosci. *22*, 106–119.

68. Wu, M., Brudzynski, S.M., and Mogenson, G.J. (1993). Functional interaction of dopamine and glutamate in the nucleus accumbens in the regulation of locomotion. Can. J. Physiol. Pharmacol. *71*, 407–413.

69. Pulvirenti, L., Swerdlow, N.R., and Koob, G.F. (1991). Nucleus accumbens NMDA antagonist decreases locomotor activity produced by cocaine, heroin or accumbens dopamine, but not caffeine. Pharmacol. Biochem. Behav. *40*, 841–845.

70. Welch, A.C., Zhang, J., Lyu, J., McMurray, M.S., Javitch, J.A., Kellendonk, C., and Dulawa, S.C. (2021). Dopamine D2 receptor overexpression in the nucleus accumbens core induces robust weight loss during scheduled fasting selectively in female mice. Mol. Psychiatry *26*, 3765–3777.

71. Södersten, P., Bergh, C., Leon, M., and Zandian, M. (2016). Dopamine and anorexia nervosa. Neurosci. Biobehav. Rev. *60*, 26–30.

72. Dang, L.C., Samanez-Larkin, G.R., Castrellon, J.J., Perkins, S.F., Cowan, R.L., and Zald, D.H. (2016). Associations between dopamine D2 receptor availability and BMI depend on age. Neuroimage *138*, 176–183.

73. Day, J.J., Roitman, M.F., Wightman, R.M., and Carelli, R.M. (2007). Associative learning mediates dynamic shifts in dopamine signaling in the nucleus accumbens. Nat. Neurosci. *10*, 1020–1028.

74. Cai, X., Liu, H., Feng, B., Yu, M., He, Y., Liu, H., Liang, C., Yang, Y., Tu, L., Zhang, N., et al. (2022). A D2 to D1 shift in dopaminergic inputs to midbrain 5-HT neurons causes anorexia in mice. Nat. Neurosci. *25*, 646–658.

75. Sotak, B.N., Hnasko, T.S., Robinson, S., Kremer, E.J., and Palmiter, R.D. (2005). Dysregulation of dopamine signaling in the dorsal striatum inhibits feeding. Brain Res. *1061*, 88–96.

76. Galmiche, M., Déchelotte, P., Lambert, G., and Tavolacci, M.P. (2019). Prevalence of eating disorders over the 2000–2018 period: a systematic literature review. Am. J. Clin. Nutr. *109*, 1402–1413.

77. Ryczko, D., and Dubuc, R. (2017). Dopamine and the brainstem locomotor networks: from lamprey to human. Front. Neurosci. *11*, 295.

78. Nieh, E.H., Vander Weele, C.M., Matthews, G.A., Presbrey, K.N., Wichmann, R., Leppla, C.A., Izadmehr, E.M., and Tye, K.M. (2016). Inhibitory input from the lateral hypothalamus to the ventral tegmental area disinhibits dopamine neurons and promotes behavioral activation. Neuron *90*, 1286–1298.

79. Corre, J., van Zessen, R., Loureiro, M., Patriarchi, T., Tian, L., Pascoli, V., and Lüscher, C. (2018). Dopamine neurons projecting to medial shell of the nucleus accumbens drive heroin reinforcement. eLife *7*, e39945.

80. Yoo, J.H., Zell, V., Gutierrez-Reed, N., Wu, J., Ressler, R., Shenasa, M.A., Johnson, A.B., Fife, K.H., Faget, L., and Hnasko, T.S. (2016). Ventral tegmental area glutamate neurons co-release GABA and promote positive reinforcement. Nat. Commun. *7*, 13697.

81. Ji, H., and Shepard, P.D. (2007). Lateral habenula stimulation inhibits rat midbrain dopamine neurons through a $GABA_A$ receptor-mediated mechanism. J. Neurosci. *27*, 6923–6930.

82. Bromberg-Martin, E.S., Matsumoto, M., and Hikosaka, O. (2010). Distinct tonic and phasic anticipatory activity in lateral habenula and dopamine neurons. Neuron *67*, 144–155.

83. Jhou, T.C., Good, C.H., Rowley, C.S., Xu, S.P., Wang, H., Burnham, N.W., Hoffman, A.F., Lupica, C.R., and Ikemoto, S. (2013). Cocaine drives aversive conditioning via delayed activation of dopamine-responsive habenular and midbrain pathways. J. Neurosci. *33*, 7501–7512.

84. Bankhead, P., Loughrey, M.B., Fernández, J.A., Dombrowski, Y., McArt, D.G., Dunne, P.D., McQuaid, S., Gray, R.T., Murray, L.J., Coleman, H.G., et al. (2017). QuPath: open source software for digital pathology image analysis. Sci. Rep. *7*, 16878.

85. Schneider, C.A., Rasband, W.S., and Eliceiri, K.W. (2012). NIH Image to ImageJ: 25 years of image analysis. Nat. Methods *9*, 671–675.

86. Bruno, C.A., O'Brien, C., Bryant, S., Mejaes, J.I., Estrin, D.J., Pizzano, C., and Barker, D.J. (2021). pMAT: an open-source software suite for the analysis of fiber photometry data. Pharmacol. Biochem. Behav. *201*, 173093.

87. Daigle, T.L., Madisen, L., Hage, T.A., Valley, M.T., Knoblich, U., Larsen, R.S., Takeno, M.M., Huang, L., Gu, H., Larsen, R., et al. (2018). A suite of transgenic driver and reporter mouse lines with enhanced brain-cell-type targeting and functionality. Cell *174*, 465–480.e22.

STAR★METHODS

KEY RESOURCES TABLE

REAGENT or RESOURCE	SOURCE	IDENTIFIER
Antibodies		
Rabbit anti-c-Fos	Cell Signaling Technology	Cat# 2250s; RRID: AB_2247211
Rabbit anti-TH	Abcam	Cat# ab112; RRID: AB_297840
Mouse anti-TH	Millipore	Cat# MAB318; RRID: AB_2201528
Guinea pig anti-Vglut2	Millipore	Cat# AB2251; RRID: AB_2665454
Rabbit anti-DsRed	Takara Bio	Cat# 632496; RRID: AB_10013483
Bacterial and virus strains		
AAV5-Ef1a-DIO-hChR2(H134R)-EYFP	Karl Deisseroth Lab	Addgene_20298
AAV-DJ8-hSyn-Con/Fon-EYFP-WPRE	Karl Deisseroth Lab	UNC GTC Vector Core #AV-2404
AAVrg-Ef1a-mCherry-IRES-Flp	Fenno et al.[40]	Addgene_55634
AAV-DJ8-CAG-Flex-WGA-EGFP	Canadian Neurophotonics Platform	SCR_016477
AAV5-hSyn-DIO-mCherry	Bryan Roth Lab	Addgene_50459
AAV1-Ef1a-Flp-DOG-NW	Tang et al.[42]	Addgene_75469
AAV8-Ef1a-Con/Fon-mCherry	Fenno et al.[40]	Addgene_137132
AAV-DJ8-CAG-DIO-EGFP-TTC	Canadian Neurophotonics Platform	SCR_016477
AAV1-Ef1a-fDIO-EYFP	Fenno et al.[40]	Addgene_55641
AAV9-hSyn-DIO-GCaMP6m	Chen et al.[46]	Addgene_100838
AAV9-hSyn-DIO-hm4D(Gi)-mcherry	Krashes et al.[49]	Addgene_44362
AAV9-hSyn-DIO-hM3D(Gq)-mCherry	Krashes et al.[49]	Addgene_44361
AAV-DJ8-Ef1a-DIO-NaChBac-EGFP	Baylor Gene Vector Core	This manuscript
AAV5-Ef1a-DIO-EYFP	Karl Deisseroth Lab	Addgene_27056
AAV9-hSyn-g-GRAB-DA3m (gDA3m)	Zhuo et al.[55]	https://doi.org/10.1101/2023.08.24.554559
AAV8-Con/Fon-GCaMP6f	Fenno et al.[47]	Addgene_137122
AAV8 -Con/Foff-GCaMP6f	Fenno et al.[47]	Addgene_137123
AAV-DJ8-Con/Fon-hM3Dq-mCherry	Baylor Gene Vector Core	This manuscript
AAV-DJ8-Con/Foff-HM3Dq-mCherry	Baylor Gene Vector Core	This manuscript
AAV-DJ8-Con/Fon-hM4Di-mCherry	Baylor Gene Vector Core	This manuscript
AAV5-DIO-Chrimson-mCherry	Klapoetke et al.[48]	Addgene_62723
AAVDJ8-FLEX-SaCas9-U6-sgVglut2	Baylor Gene Vector Core	This manuscript
AAVDJ8-FLEX-SaCas9-U6-sgRNA	Baylor Gene Vector Core	This manuscript
Chemicals, peptides, and recombinant proteins		
Clozapine N-oxide (CNO)	Sigma-Aldrich	#C8032
Formalin	Fisher	#SF100-4
Tetrodotoxin (TTX)	Alomone labs	#T-550
4-Aminopyridine (4-AP)	Sigma-Aldrich	#A78403
Dinitroquinoxaline (DNQX)	Tocris	#0189
DL-AP5	Tocris	#0105
Critical commercial assays		
RNAscope® Multiplex Fluorescent Detection Kit v2	Advanced Cell Diagnostic	#323270
Deposited data		
https://doi.org/10.17632/whpdth36pr.1	Mendeley data	N/A

(*Continued on next page*)

Continued

REAGENT or RESOURCE	SOURCE	IDENTIFIER
Experimental models: Organisms/strains		
Mouse: Vglut2-Cre	The Jackson Laboratory	IMSR_JAX:016963
Mouse: Vgat-Flp	The Jackson Laboratory	IMSR_JAX:031331
Oligonucleotides		
RNAscope® Probe - Mm-Slc32a1	Advanced Cell Diagnostic	#319191
RNAscope® Probe - Mm-Fos-C2	Advanced Cell Diagnostic	#316921-C2
Recombinant DNA		
pAAV-nEF Con/Fon DREADD Gq-mCherry	Karl Deisseroth Lab	Addgene_183532
pAAV-nEF Con/Foff DREADD Gq-mCherry	Karl Deisseroth Lab	Addgene_183533
pAAV-nEF-Con/Fon DREADD Gi-mCherry	Karl Deisseroth Lab	Addgene_177672
pAAV-FLEX-SaCas9-U6-sgRNA	Hunker et al.[63]	Addgene_124844
pAAV-FLEX-SaCas9-U6-sgSlc17a6	Hunker et al.[63]	Addgene_124847
Software and algorithms		
pClamp	Molecular Devices	RRID:SCR_011323; http://www.moleculardevices.com/products/software/pclamp.html
GraphPad Prism (9.5.1)	GraphPad	RRID:SCR_002798; http://www.graphpad.com/
Ethovision XT 11.5	Noldus	https://www.noldus.com/ethovision-xt
Qupath 0.4.3	Bankhead et al.[84]	https://qupath.readthedocs.io/en/0.4/
ImageJ 1.54D	Schneider et al.[85]	https://imagej.net
Doric Neuroscience Studio v6.1.2.0	Doric Lenses	https://neuro.doriclenses.com/products/doric-neuroscience-studio
pMat	Bruno et al.[86]	https://github.com/djamesbarker/pMAT
Matlab R2023a	Mathworks	https://www.mathworks.com/?s_tid=gn_logo

RESOURCE AVAILABILITY

Lead contact

Further information and requests for resources and reagents should be directed to and will be fulfilled by the lead contact, Qingchun Tong (qingchun.tong@uth.tmc.edu).

Materials availability

This study did not generate new unique reagents.

Data and code availability

- All original data has been deposited at Mendeley and is publicly available as of the date of publication. The DOI is listed in the key resources table.
- This paper does not report original code.
- Any additional information required to reanalyze the data reported in this paper is available from the lead contact upon request.

EXPERIMENTAL MODEL AND STUDY SUBJECT DETAILS

Animal care and procedures were approved by the University of Texas Health Science Center Houston Institutional Animal Care and Use Committee. Mice were housed at 21–22 °C on a 12 h light/12 h dark cycle with standard pellet chow and water ad libitum otherwise noted for fasting experiments, calorie-restricted diet for nosepoke training or high fat diet treatment. Mice were group-housed most of the time and singly-housed for measurement of daily food intake or housed in metabolic cages. Vglut2-Cre and Vgat-Flp mice were purchased from The Jackson Laboratory (strain no. 016963 and no. 031331) and described previously.[39,87] Male and female mice were used in preliminary study and key functional studies and no significant difference was revealed. Mice used in experiments were acquired from same litters in different treatment groups and were 7∼16 weeks old when used for surgery purposes.

METHOD DETAILS

Stereotaxic surgery

The delivery of viral vectors and implantation of optic cannulas were conducted through stereotaxic surgeries. Mice were anesthetized with a ketamine/xylazine cocktail (100 mg/kg and 10 mg/kg, respectively, intraperitoneal), and their heads were affixed to a stereotaxic apparatus in absence of the pedal reflex. Viral vectors were delivered through a 0.5 μL syringe (Neuros Model 7000.5 KH, point style 3; Hamilton, Reno, NV, USA) mounted on a motorized stereotaxic injector (Quintessential Stereotaxic Injector; Stoelting, Wood Dale, IL, USA) at a rate of 30 nL/min. Viral preparations were titered at ~10^{12} particles/mL. Volumes and coordinates for viral injections were as follows: 50~75 nl/side, anteroposterior (AP) +1.25 mm, mediolateral (ML) ±0.2 mm, dorsoventral (DV) -4.95 mm for the BF; 50~75 nl/side, AP -3.1 mm, ML ±0.3 mm, DV -4.6 mm for the VTA; 100 nl/side, AP +1.4 mm, ML -1.0 mm, DV -4.5 mm for the NAc. For optogenetic experiments, customized fiber optic cannulas [Ø1.25-mm stainless ferrule, Ø200-μm core, 0.39 numerical aperture (NA), 4.7 mm; Inper, Zhejiang, China] were implanted to target the VTA (AP -3.1 mm, ML -0.3 mm, DV -4.4 mm). For fiber photometry experiments, customized wide-aperture fiber optic cannulas (Ø1.25-mm stainless ferrule, Ø400-μm core, 0.66 NA, 5.0 mm; Doric Lenses, Quebec, QC, Canada) were implanted in the BF (AP +1.2 mm, ML -0.2 mm, DV -4.7 mm), the VTA (10°, AP -3.1 mm, ML -0.3 mm, DV -4.7 mm) and the NAc (10°, AP +1.4 mm, ML -1.7 mm, DV -4.2 mm). For AP5 and CNQX *in vivo* infusions, an optofluid cannula with interchangeable injectors (M3, Ø200-μm core, 0.37 NA, 4 mm guiding tube, 4.7 mm fiber, 4.5 mm injector; Doric Lenses, Quebec, QC, Canada) was implanted in the VTA. For all cannula implants, fibers were fixed to the skull with glue and dental cement (Stoelting 51458; Stoelting co., IL, USA). For the following three days of neurosurgery, mice were treated with Caprofen (Rimadyl; Zoetis Inc, MI, USA; i.p., 5mg/kg) for pain relief.

Brain slice electrophysiological recordings

Electrophysiological recordings were performed as previously described. Briefly, 4-6 weeks after AAV infusion, mice were deeply anesthetized with Isoflurane (NDC 66794-017-10), and the brain was quickly removed. Coronal slices (280 μm) containing the basal forebrain or VTA were cut in oxygenized, ice-cold artificial cerebrospinal fluid (aCSF) containing (in mM): 123 NaCl, 26 $NaHCO_3$, 2.5 KCl, 1.25 NaH_2PO_4, 10 glucose, 1.3 $MgCl_2$, 2.5 $CaCl_2$ bubbling with 95% O_2/5% CO_2 with a Leica VT1000S vibratome. Slices were incubated at 31-32 °C for 30 min and maintained at room temperature for at least 1 hour to allow for recovery before any electrophysiological recordings.

Individual slices were then transferred to a recording chamber mounted on an upright microscope (Olympus BX51WI) and continuously superfused (2 mL/min) with aCSF maintained at 32-34 °C by passing it through a feedback-controlled in-line heater (TC-324B; Warner Instruments). Cells were visualized through a 40X water-immersion objective with differential interference contrast (DIC) optics and infrared illumination. Fluorescent-guided whole-cell patch clamp recordings were performed with a MultiClamp 700B amplifier (Axon Instruments). Patch pipettes were 3–5 MΩ when filled with an internal solution containing (in mM): 142 K-gluconate, 10 HEPES, 1 EGTA, 2.5 $MgCl_2$, 0.25 $CaCl_2$, 4 Mg-ATP, 0.3 Na-GTP, 10 Na_2-Phosphocreatine (pH 7.3 adjusted with KOH, 300 mOsmol).

To activate ChR2, light from a 473 nm laser (Opto Engine LLC, Midvale, UT, USA) was focused on the area of the recorded VTA neurons to produce spot illumination through optic fiber. Brief pulses of light (2-5 ms duration, 2-4 MW/mm^2) were delivered under the control of acquisition software. Tetrodotoxin (TTX, 0.5 μM, Alomone labs, Jerusalem, Israel), and 4-Aminopyridine (4-AP, 100 μM, Sigma-Aldrich, St. Louis, MO, USA) were bath-applied during voltage-clamp recordings to block action potential and network activity to verify the monosynaptic connection.

Fiber photometry

All fiber photometry recordings were conducted using a Doric Lenses setup, with a light-emitting diode (LED) driver controlling two connectorized LEDs (405, 465) routed through a 5-port Fluorescence MiniCube or a 7-port Flurescence Minicube with a specific port for red opsin activation to deliver excitation light for isosbestic and calcium or dopamine-dependent signals, or for red opsins to the implanted optic fiber simultaneously. Emitted light was collected by the same fiber and focused onto separate photoreceivers (Newport 2151) based on the wavelength pf fluorescent light. A Doric Fiber Console controlled by the Doric Studios (V6.1.4.0) was used to control the LEDs, photostimulation lasers, and demodulate the collected signals based on the wavelength.

For dual-cannula recordings in the BF and the VTA, we used the following experimental procedure. Animals were habituated in the recording cage for 10 minutes with the optic fiber connected. After habituation, signals and mice behaviors were recorded for 10 minutes. The first stimulus was delivered 2 minutes post recording initiation and each stimulus was given at least 1 minute apart. The water spray, air puff and object drop were presented to mice on different dates, at least three days apart.

For single-cannula dopamine recordings in the NAc, we used the following experimental procedure. Animals were habituated in the recording cage for 10 minutes with the optic patch fiber connected. After habituation, signals and mice behaviors were recorded for 10 minutes. The first stimulus (water spray or photostimulation (λ = 473 nm, 20 Hz, 20 ms, 10 s or 20 s) was delivered 2 minutes post recording initiation and each stimulus was given at least 1 minute apart. For the photostimulation assay, the photostimulation was applied to the VTA cannulas, and LEDs were applied to the NAc cannulas. For feeding assay, chow diet-fed mice which had been pre-exposed to HFD were given the free access to HFD. The mice were habituated in the recording cage for 10 minutes with the presence of HFD pellets. For feeding assay with photostimulation, mice were also exposed to and given the free access to HFD

pellets. Yet, during 10-min recording epochs, once the mice engaged with feeding, the photostimulation (20 Hz, 20 ms, 10 s) was applied to a separate optic cannula implanted in the VTA.

For single-cannula recordings and photostimulation in the VTA, we used the following experimental procedure. The photostimulation laser and LEDs were applied to the same optic cannula in the VTA. Animals were habituated in the recording cage for 10 minutes with the optic patch cable connected. After habituation, signals and mice behaviors were recorded for 10 minutes. The first photostimulation sequence (λ = 638 nm, 20 Hz, 20 ms, 10 s) was delivered at 50 seconds and followed by another 4 sequences with 50 seconds apart from each other.

In vivo photostimulation

Behavioral measurements were performed during the light cycle of the day at least four weeks post-surgery. An integrated rotary joint patch cable (Doric Lenses, Quebec, QC, Canada) was used to connect the ferrule of the implanted optic fiber to the 473-nm diode-pumped solid-state laser (Opto Engine LLC, Midvale, UT, USA). Light pulses (20 Hz, 20 ms) were controlled by Master-8 pulse stimulator (A.M.P.I., Jerusalem, Israel). Mice were placed in the sanitized Phenotyper cages (Noldus, Wageningen, Netherlands) with a camera real-time recording on top of the cage. After each test, cages were cleaned and sanitized with 75% ethanol. Before behavioral tests, mice were acclimated in the behavior room for at least 30 min.

Real-time place avoidance (RTPA)

The Noldus Phenotyper chamber was divided into two halves, one of which was paired with photostimulation. Mice were placed in the laser-off side in the beginning and were free to roam in the enclosure. The EthoVision XT software (version 15.0; Noldus) was triggered to collect tracking data for 10 minutes when mice entered the side paired with the photostimulation and the light pulses were applied. RTPA was repeated with the side paired with photostimulation counterbalanced after a week.

Fasting refeeding assay

Mice were fasted overnight (16∼18 hours). Chow diet pellets were placed in a petri dish in a corner of Phenotyper cages. Mice were put in the center of cage and were free to roam in the enclosure. Once the mice entered the food corner and engaged in feeding, the Ethovision XT software was triggered to collect tracking data and apply laser pulses for 10 minutes. The weight of pellets consumed during the 10 minutes experiment episode were recorded. To deliver the glutamate receptor antagonists, the optic fiber cannula was removed from the guiding cannula and the injector was inserted. A syringe (0.5 μL, Model 7000.5KH, 25 ga, 2.75 in) joined with a plastic tube (RenaSil Silicone Rubber Tubing,.025 OD X.012 ID; Braintree Scientific, INC, Braintree, MA, USA) was used to deliver 50 nL (61 mM D-AP5 solution in saline) + 50 nL (24 mM DNQX solution in 25–30% DMSO) cocktail. After 5 minutes incubation, the injector was removed, and the optic cannula was re-inserted, followed by feeding assays as described above.

Laser on-off open field test

Mice were put in the center of Phenotyper cages and were acclimated for three minutes before the software tracking. Mice were free to roam in the enclosure and underwent 15-min trials consisting of three consecutive 5-min epochs (pre-laser, laser-on, and post-laser). During pre-laser and post-laser epochs, the laser was turned off. During the laser-on period, the laser (20 Hz, 20 ms) was applied. The total distance travelled, and the time spent in different zones were collected.

Chemogenetics

Mice that received hM3Dq or hM4Di viral vectors and control mice were treated with either saline or Clozapine-N-oxide (1 mg/kg, i.p.). Behavioral tests were conducted 30 min post injections. For each cohort, half of mice were injected with saline and half of the mice were injected with CNO. After one week, experiments were repeated mice with saline and CNO injections in a counterbalance fashion. For metabolic cages recordings, mice were acclimated in metabolic cages for 2 days before application of saline/CNO at ZT 6.

Singly housed fasting refeeding assay

Mice were singly housed and overnight fasted (16∼18 hours) or 6-hour fasted at the light cycle before the assay. Mice were provided with standard chow pellets 30 min after saline/CNO application. Food pellets were weighed at 0 h, 0.5 h, 1 h, 2 h, 4 h, and 6 h after mice accessed the food pellets.

Operant conditioning

Mice were singly housed and kept with a calorie-restricted diet that they maintained 80∼85% of their original body weight for a week prior to training. Mice were trained daily for 30 min in Nose Poke chambers (Nose Poke chambers, MED-307W-B2, Med Associates Inc, Fairfax, VT) on gradually-increasing fixed ratios (FR) of 1, 5, and 15. FR was increased whenever mice were able to acquire 25 pellets within 30 min. At the test day, mice from both groups were injected with CNO and tested for positive reinforcements. Three days later, mice were tested again with saline injections.

HFD preference test

Mice were habituated to HFD for three days before the testing day. At the testing day, animals were fasted for 6 hours at the light cycle to induce feeding behaviors and were placed in the Noldus chamber. In the chamber, two petri dishes with respective HFD and CD were placed in two different corners of the chambers, and two empty dishes were placed in the other two corners. Mice were allowed to freely access any corner for 10 minutes and consumption of HFD and CD was recorded.

LDT and OFT

In LDT and OFT experiments, mouse movement was recorded with cameras mounted on top of the maze, the box and the phenotyper and tracked for 10 minutes using Ethovision XT software. The duration and frequency to access open arms, the light side chamber and the center of chamber were collected. For individual mice that went through consecutive tests in weeks, the order was LDT and then OFT.

Physiology assessment

Metabolic cages

Mice were individually housed in chambers of Columbus Instruments Comprehensive Lab Animal Monitoring System (Columbus Instruments, Columbus, Ohio, USA) for chemogentic experiments or the PhenoMaster cages (TSE systems, Chesterfield, Missouri, USA) for long-term body weight monitoring experiments. Mice were given ad libitum access to a normal chow diet and water. Food intake, O2 consumption, and locomotion activity levels were measured using indirect calorimetry continuously at different time points. Data was averaged through different time points in light and dark cycles, respectively, for comparison. The data from the first day and the last day was removed.

Body weight and food intake measurement

Long-term body weights were collected weekly for 8 weeks post-surgery under normal chow diet and for another 8 weeks under high-fat diet (Research Diets D12492; 20% protein, 60% fat, 20% carbohydrate, 5.21 kcal/g). *Ad libitum* food intake was measured at the end of metabolic cages assessment and mice were singly housed. Daily food intake was recorded and averaged for three days.

Post-hoc analysis

Perfusion and tissue dissection

To harvest brain tissues, mice were anesthetized with ketamine/xylazine (150 mg/kg and 15 mg/kg, respectively). After loss of the pedal reflex, mice were transcardially perfused with 15 ml of saline and 15 ml of 10% buffered formalin (In Vivo Perfusion System IV-140, Braintree Scientific Inc.). The brains were then collected and stored in 10% buffered formalin overnight at room temperature, and then, the brain was switched to 30% sucrose in PBS for overnight. Brains were sectioned into 30 μM coronal slices on a frozen sliding microtome and stored in 0.1% NaN3 in PBS at 4 °C.

Immunohistochemistry (IHC)

For IHC, sectioned slices were rinsed with 0.3% Triton X-100 in phosphate-buffered saline (PBS) for 5 min three times and were blocked in 0.3% Triton X-100 in PBS with 10% donkey serum at room temperature (RT) for 1 hour. The slices were incubated in a primary antibody solution (primary antibody, 5% donkey serum, and 0.3% Triton X-100 in PBS) overnight at 4°C. The following primary antibodies were used: c-Fos rabbit monoclonal antibody (mAb) (9F6) (1:1000, #2250; Cell Signaling Technology), tyrosine hydroxylase rabbit polyclonal antibody (1:1000, ab112; abcam). For secondary antibody treatment, slices were rinsed with 0.3% Triton X-100 in PBS for 5 min for three times and incubated in the secondary antibody solution (Alexa Fluor 647–conjugated AffiniPure Donkey (H+L) anti-rabbit immunoglobulin G (Jackson ImmunoResearch), 1:400, 10% donkey serum, and 0.3% Triton X-100 in PBS) for 2 hours at RT. The floating slices were mounted onto microscope slides and coverslipped with Fluoromount (Diagnostic BioSystems Inc., Sigma-Aldrich). A confocal microscope was used to image the slices at different resolutions (Leica TCS SP5, Leica Microsystems, Wetzlar, Germany). Mice with offsite injections and cannula implants were removed from the study. The confocal images were processed with ImageJ 1.54D.[85] The fluorescence-positive neurons were recognized and quantified in the software QuPath 0.4.2 (https://qupath.github.io).[84]

In situ *hybridization (ISH)*

For in situ hybridization experiment to detect mRNA levels, fixed-frozen brain tissues were sectioned at 17.5 μm thickness using a sliding microtome and mounted onto Superfrost Plus Gold slides (Fisher Scientific, INC). Sections were first air dry at RT for 30 minutes and baked at 60 °C for 30 minutes. Sections were post-fixed with pre-cold 10% neutral buffered formalin at 4 °C for 15 minutes. Sections were further dehydrated with 50%, 70%, and 100% ethanol at RT and then applied with 3% hydrogen peroxide for 10 minutes at RT. After 10 minutes' antigen retrieval at 98∼100 °C, sections were digested with protease (RNAscope™ Protease III, #322340, Advanced Cell Diagnostic, INC). Sections were hybridized with probes against Vgat (RNAscope® Probe - Mm-Vgat, # 319191, Advanced Cell Diagnostic, INC) and Fos (RNAscope® Probe - Mm-Fos-C2, #316921-C2, Advanced Cell Diagnostic, INC) for 2 h at 40 °C and signals were amplified with RNAscope® Multiplex Fluorescent Reagent Kit v2 with TSA Vivid Dyes (#323270, Advanced Cell Diagnostic, INC). The fluorescence-positive neurons were recognized and quantified in the software QuPath 0.4.2 (https://qupath.github.io).

QUANTIFICATION AND STATISTICAL ANALYSIS

GraphPad Prism 9.5.1 (GraphPad Software, Inc., La Jolla, CA, USA) was used for all statistical analyses and construction parts of the figures. For fiber photometry data, raw data from single trials was first processed through pMat application (https://github.com/djamesbarker/pMAT).[86] Individual traces were aligned to zero at stimulus onset and averaged to be visualized in MATLAB R2022b (student version). In the heatmaps, signals were normalized from 0 to 1 across each trial. The unpaired two-tailed Student's t-test was used for single-variable comparisons. Two-way repeated ANOVA followed by Sidak's multiple comparisons were used for repeated measurements in group comparisons. Two-way non-repeated ANOVA followed by Sidak's multiple comparisons was used for group comparisons. Error bars in graphs were represented as mean ± s.e.m. $p < 0.05$ was considered significant. $p^* < 0.05$, $p^{**} < 0.01$, $p^{***} < 0.005$, $p^{****} < 0.0001$. The sample sizes were chosen based on previously published work. All tests met assumptions for normal distribution, with similar variance between groups that were statistically compared. N values represent the final number of animals used in experiments following genotype verification and post-hoc validation of injection sites/cannula implantations.